Original research

Antibody-induced erythrophagocyte reprogramming of Kupffer cells prevents anti-CD40 cancer immunotherapy-associated liver toxicity

Marc Pfefferlé,[1] Irina L Dubach,[1] Raphael M Buzzi,[1] Elena Dürst,[1] Nadja Schulthess-Lutz ![ORCID],[1] Livio Baselgia,[1] Kerstin Hansen,[1] Larissa Imhof,[1] Sandra Koernig,[2] Didier Le Roy,[3] Thierry Roger,[3] Rok Humar,[1] Dominik J Schaer,[1] Florence Vallelian ![ORCID] [1]

[1]University of Zurich, Zurich, Switzerland
[2]CSL Ltd., Research, Bio21 Institute, Parkville, Victoria, Australia
[3]University of Lausanne, Lausanne, Switzerland

Correspondence to
Dr Florence Vallelian;
florence.vallelian@usz.ch

ABSTRACT

Background Agonistic anti-CD40 monoclonal antibodies (mAbs) have emerged as promising immunotherapeutic compounds with impressive antitumor effects in mouse models. However, preclinical and clinical studies faced dose-limiting toxicities mediated by necroinflammatory liver disease. An effective prophylactic treatment for liver immune-related adverse events that does not suppress specific antitumor immunity remains to be found.

Methods We used different mouse models and time-resolved single-cell RNA-sequencing to characterize the pathogenesis of anti-CD40 mAb induced liver toxicity. Subsequently, we developed an antibody-based treatment protocol to selectively target red blood cells (RBCs) for erythrophagocytosis in the liver, inducing an anti-inflammatory liver macrophage reprogramming.

Results We discovered that CD40 signaling in Clec4f^{+} Kupffer cells is the non-redundant trigger of anti-CD40 mAb-induced liver toxicity. Taking advantage of the highly specific functionality of liver macrophages to clear antibody-tagged RBCs from the blood, we hypothesized that controlled erythrophagocytosis and the linked anti-inflammatory signaling by the endogenous metabolite heme could be exploited to reprogram liver macrophages selectively. Repeated low-dose administration of a recombinant murine Ter119 antibody directed RBCs for selective phagocytosis in the liver and skewed the phenotype of liver macrophages into a Hmox^{high}/Marco^{high}/ MHCII^{low} anti-inflammatory phenotype. This unique mode of action prevented necroinflammatory liver disease following high-dose administration of anti-CD40 mAbs. In contrast, extrahepatic inflammation, antigen-specific immunity, and antitumor activity remained unaffected in Ter119 treated animals.

Conclusions Our study offers a targeted approach to uncouple CD40-augmented antitumor immunity in peripheral tissues from harmful inflammatoxicity in the liver.

WHAT IS ALREADY KNOWN ON THIS TOPIC

⇒ Inflammatoxicity in the liver is a dose-limiting adverse activity of anti-CD40-based cancer immunotherapy. Established immunosuppressive and anti-inflammatory drugs like glucocorticoids and TNF-blocking agents can effectively suppress liver-inflammation, but may undermine antitumor efficacy. Novel strategies to prevent liver-toxicity focused on either liver-specific anti-inflammatory functions or targeting CD40-activity towards extrahepatic antigen-presenting cells.

WHAT THIS STUDY ADDS

⇒ We identified Kupffer cells as the essential driver of anti-CD40-induced liver toxicity, setting the stage for a selective strategy to prevent immunotherapy induced liver toxicity. Based on this pathophysiological insight, we developed a monoclonal antibody-based protocol to direct host erythrocytes for phagocytosis in the liver, inducing liver-restricted anti-inflammatory macrophage reprogramming. With this conditioning strategy, we could uncouple anti-CD40-stimulated inflammation and immunity in the liver and in extrahepatic tissues.

HOW THIS STUDY MIGHT AFFECT RESEARCH, PRACTICE OR POLICY

⇒ Our study provides proof of concept for liver selective anti-inflammatory macrophage reprogramming, which may support the development of more effective and less harmful immunotherapy protocols in cancer medicine.

tumors when combined with chemotherapy, radiotherapy, or other immunotherapies.[1–4] CD40 ligation and activation drive not only T-cell-dependent[5–9] but also T-cell-independent antitumor immunity, such as the reprogramming of tumor-associated macrophages into antitumor macrophages.[10 11]

BACKGROUND

Agonistic anti-CD40 monoclonal antibodies (mAbs) have shown strong immunotherapeutic effects in preclinical models of solid

CD40 targeting employs an agonistic immunotherapeutic strategy. In contrast to immune checkpoint-inhibiting antibodies, which block intrinsic receptor–ligand interactions, agonistic compounds must be carefully dosed to reach efficiency without triggering harmful side effects. Systemic administration of agonistic anti-CD40 mAb leads to the activation of macrophages in multiple organs, producing cytokine release syndrome and, notably in the liver, leading to necroinflammatory liver injury.[12] Liver toxicity is currently the main factor limiting the use of anti-CD40 mAbs at higher and more anti-tumor effective doses in clinical settings. This has been demonstrated in mouse models, in which anti-CD40 mAbs were delivered intravenously at high doses (5–20 mg/kg).[12–15] When improperly administered before chemotherapy, anti-CD40 treatment can result in lethal hepatotoxicity in mice.[14] In humans, clinical trials of anti-CD40 mAb administration reported a mild to moderate elevation in transaminase levels, even when anti-CD40 mAbs were applied at low doses (0.1–0.2 mg/kg).[16–18] Although less frequent, liver toxicity has also been reported as an immune-mediated adverse effect of other immunotherapies, including checkpoint inhibitors.[19] Glucocorticosteroids and TNF-blocking agents have been successfully used to treat immune-related adverse events (irAEs) induced by immunotherapeutic agents in cancer treatment.[20 21] However, the systemic anti-inflammatory and immunosuppressive activity of these drugs may negatively affect their antitumor efficiency.[22–25] To fully leverage the antitumor potential of anti-CD40 mAbs and other immunotherapeutic agents, a specific prophylactic treatment for liver irAEs that does not suppress antitumor immunity remains to be found.

Mechanistically, anti-CD40 mAbs induce hepatotoxicity by stimulating localized cytokine expression and reciprocal immune-cell activation in the liver, including lymphocytes, Kupffer cells, neutrophil granulocytes, and endothelial cells.[12 13] Moreover, lineage selective conditional knockout of CD40 in all macrophages throughout the body abrogated the disease.[12] These data suggest that CD40-ligation on Kupffer cells could be an indispensable trigger of liver disease, rationalizing the development of therapeutic interventions to selectively reprogram liver macrophages into an anti-inflammatory phenotype.

One of the most archetypical functions of resident liver macrophages is the clearance of membrane-altered or antibody-tagged red blood cells (RBCs) during hemolytic stress.[26] In mice with genetic spherocytosis or phenylhydrazine-induced hemolytic anemia, we have discovered that phagocytosis of RBCs and subsequent heme signaling through the transcription factor NRF2 transformed liver macrophages into erythrophagocytes with a profoundly attenuated inflammatory response on activation of CD40 and TLR signaling pathways.[27–29] Based on these observations, we hypothesized that therapeutic targeting of RBCs with an opsonizing mAb could selectively induce erythrophagocyte transformation in the liver, resulting in an anti-inflammatory mode of action with unique liver tropism.

Here, we exploited time-resolved single-cell RNA-sequencing (scRNA-seq) and Kupffer cell selective conditional gene knockout to demonstrate that CD40 signaling in resident liver macrophages is indeed the principal upstream trigger of anti-CD40 mAb-induced liver toxicity. We then used a recombinant antibody targeting RBCs for erythrophagocytosis to induce selective erythrophagocyte reprogramming of liver macrophages before administering high-dose agonistic anti-CD40 mAb. This conditioning strategy allowed us to uncouple antitumor immunity in peripheral tissues from harmful inflammatoxicity in the liver. Based on these data, antibody-instructed erythrophagocyte transformation may evolve as a liver-selective anti-inflammatory strategy in cancer immunotherapy and potentially other inflammatory and metabolic liver diseases.

METHODS

Mouse strains and treatment protocols

Details about mouse strains, treatment protocols, tissue sampling, and single cell preparation can be found in online supplemental methods sections. Rat anti-mouse Ter119 IgG2 mAb was acquired from InVivoPlus and diluted in sterile phosphate-buffered saline (PBS) before s.c. injection. Murine Ter119 (mTer119) IgG2 mAb was produced by CSL Behring[30] (non-commercialized) and diluted in sterile PBS before s.c. injection.

Agonistic anti-CD40 mAb challenge

Anti-CD40 mAbs were purchased from BioXCell (clone FGK4.5/FGK45) and injected intravenously at 20 mg/kg in a maximum volume of 5 µL/g weight. Animals were sacrificed 16 hours later for cytokine and macrophage gene expression measurement or 30 hours later for plasma alanine aminotransferase (ALT) measurement, liver histology, and colon histology.

Histology

Detailed protocols for tissue preparation, staining and imaging can be found in online supplemental methods sections. Whole-liver sections processed by H&E, immunohistochemical or immunofluorescence (IF) staining, and embedded in paraffin were acquired using a Zeiss Axio Scan.Z1 and Akoya Phenoimager HT microscope. Regions of liver vibratome sections subjected to IF staining were visualized with a Leica SP8 confocal laser scanning microscope. Images were analyzed using Qupath[31] (V.0.3.2) and ImageJ.

Macrophage quantification in IF tissue sections

F4/80+ cells were quantified in whole-liver sections using the integrated watershed cell detection plugin in Qupath. The cells were detected in the Alexa Fluor 555 channel using a requested pixel size of 0.5 µm. The background radius, median filter radius and sigma were 8, 0 and

1.5 µm, respectively. The minimum and maximum areas were 10 and 400 µm², respectively. The threshold was set to 150, and cell expansion to 2 µm.

Flow cytometry

In all flow cytometry experiments, except for flow cytometric analysis of RBCs, live dead staining was performed using the LIVE/DEAD Fixable Near-IR cell stain kit (Invitrogen) as described by the manufacturer. Fc receptor blockade was performed by preincubating cells with TruStain FcX PLUS (anti-mouse CD16/32) antibodies (BioLegend). Multiparameter analysis was performed with an LSR Fortessa analyzer (BD Biosciences) or an Aurora 5 L spectral flow cytometer (Cytek). The autofluorescence of cells was subtracted in all experiments using a spectral flow cytometer. Data were analyzed using FlowJo software (V.10.7.1) and flow cytometry software express V.6 (De Novo software).

Bone marrow-derived macrophages cell culture

Bone marrow (BM) cells were isolated by flushing the femurs and tibias of 8–10-week-old C57BL/6J mice, followed by straining of the BM through a 70 µm filter. The BM cells were plated at a density of 30,000 cells/cm² on tissue culture-treated 96-well plates (TPP) in complete RPMI-1640 medium (10% FCS and 1% L-glutamine) supplemented with 1% penicillin/streptomycin and 100 ng/mL recombinant mouse M-CSF (PeproTech). On day 3, half of the medium was replaced. Experiments were carried out on day 7.

In vitro erythrophagocytosis assay

BM-derived macrophages (BMDMs) were isolated and cultured on a 96-well plate at a concentration of 10^4 cells/well as described above. On day 7 of BMDM culture, donor RBCs were obtained from mice by submental vein puncture. The whole-blood samples were washed twice with PBS. RBCs (50×10^6) were stained using red pHrodo (pHrodo Cell Labeling Kit for Incucyte Phagocytosis Assays, Sartorius) according to the manufacturer's protocol. Stained RBCs were added to increasing concentrations of BMDMs. Immediately before starting image acquisition, the Ter119 antibody (400 µg/mL) was added to each well. Images were acquired every 15 min for 8 hours using an Incucyte live-cell analysis system.

Sequencing-based workflows and data analysis

Detailed description of the workflow for scRNAseq experiments using the 10x Genomics Chromium platform, Illumina sequencing, and data analysis are provided in online supplemental methods section. Sequencing data can be accessed at the Gene Expression Omnibus under accession no. GSE202918.

RT-qPCR analysis

The experimental details for RNA isolation, cDNA synthesis, qPCR, and primer sequences are provided in online supplemental methods section.

Statistical analysis

Sample size was calculated with R (V.4.1.2). Data plotting and statistical analysis were performed with Prism V.9 (GraphPad) and JMP V.15 (SAS) or the Bioturing Single-Cell browser (V.3.3.15). We used analysis of variance with Tukey's post-test, t-tests (two tailed), and Fisher's exact test or χ^2 test to analyze contingency tables, as indicated in the figure legends. All data points are displayed in bar plots as the mean±SD (n.s.=not significant, *p≤0.05, **p≤0.01, ***p≤0.001, ****p≤0.0001).

RESULTS

Kupffer cell activation drives anti-CD40 mAb-induced liver inflammatoxicity in mice

To identify a cell target for the selective suppression of anti-CD40 mAb-induced liver toxicity, we studied the sequence of inflammatory processes leading to liver toxicity due to anti-CD40 treatment. To this end, we used our previously described mouse model of anti-CD40 mAb-induced necroinflammatory liver disease.[12] Consistent with our previously published results, thirty hours after intravenous injection of anti-CD40 mAb, we detected large areas of liver necrosis by histology (figure 1A) and a significant increase in liver enzyme (ALT) levels in plasma, indicating liver toxicity (figure 1B). The administration of anti-CD40 mAb also induced a systemic inflammatory cytokine response starting 7 hours postinjection which then peaked at 24 hours postinjection (figure 1C). We then performed a time-resolved scRNA-seq experiment with CD45-enriched liver cell suspensions that were isolated from saline-treated mice (0 hour) and anti-CD40-treated mice at 7 hours, 14 hours, or 22 hours after administration. Cells from each condition were labeled with DNA-barcoded antibodies, pooled and processed for sequencing (figure 1D). Figure 1E shows a uniform manifold approximation and projection plot containing merged data from the cells across the four treatment time points. The cellular identity of each cell cluster was determined by matching its gene expression profile with canonical marker genes for Kupffer cells, monocytes, neutrophils, dendritic cells, T and B lymphocytes, and endothelial cells (figure 1F, online supplemental figure 1A,B) and the cell population dynamics was analyzed over time (figure 1G and online supplemental figure 2). At baseline, we found primarily an endothelial cell population and a population of Clec4f⁺ Kupffer cells. At 7 hours, we detected a position shift in the Clec4f⁺ Kupffer cell population. This shift reflected an inflammatory transformation of the Kupffer cells, accompanied by the induction of the expression of multiple chemokines, including Cxcl9 and Cxcl10, and a strong signal for the activated IFN alpha and IFN gamma signaling pathways based on gene set enrichment analysis (GSEA) (figure 1H, online supplemental figure 3A,B). At 14 hours, the liver leucocyte population was dominated by recruited Ly6c2⁺ monocytes. The strong expression of Ccr2 in monocytes observed at 14 hours paired with the expression of Ccl2
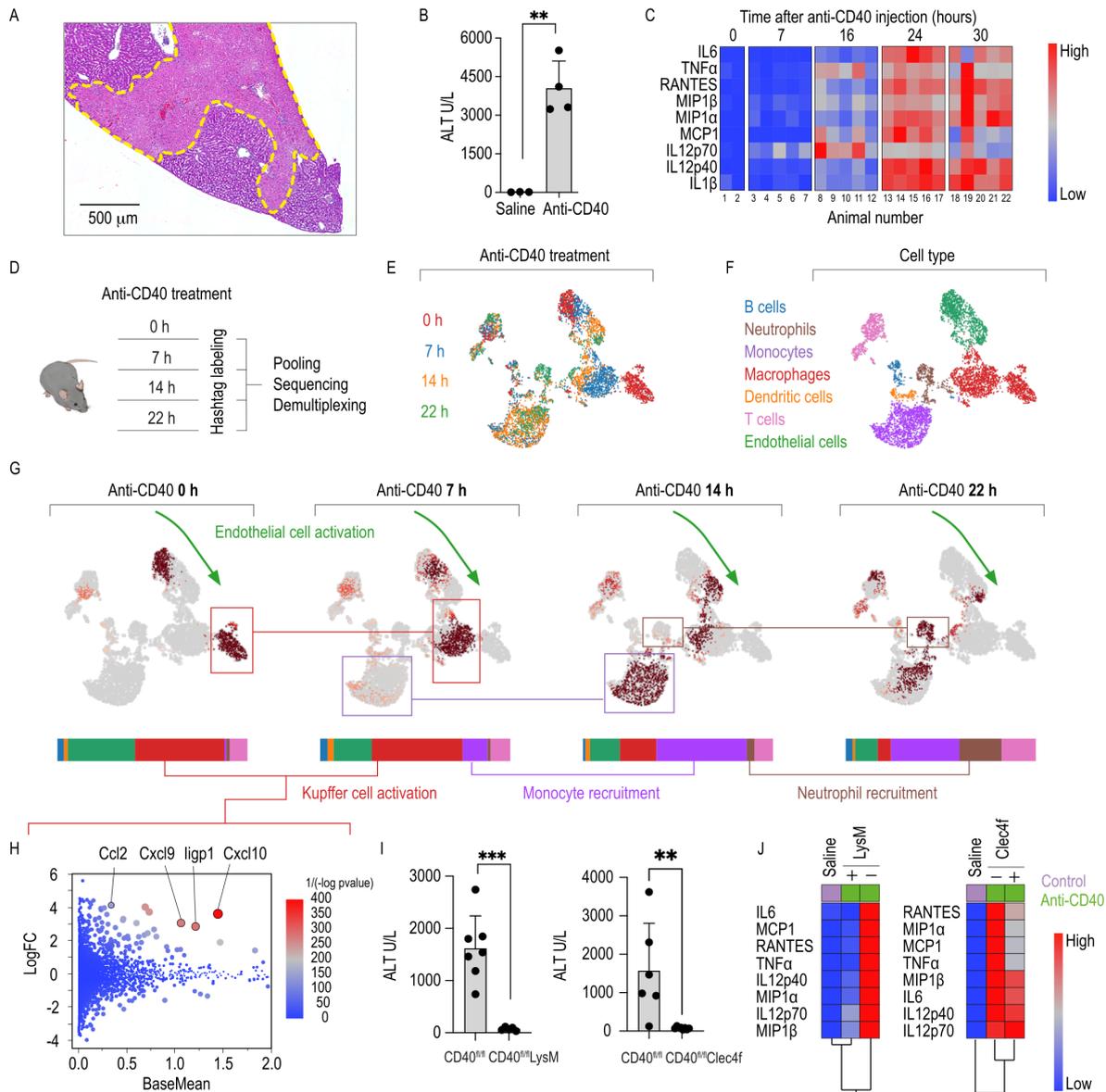
Figure 1 Anti-CD40 mAb treatment drives hepatotoxicity which requires Kupffer cell activation as the essential primary hit. (A) Representative image of a liver section stained with H&E from a C57BL/6 mouse harvested at 30 hours after intravenous injection of an agonistic anti-CD40 mAb (20 mg/kg). Dotted lines show the boundary between necrotic and healthy tissue. (B) Bar plots displaying plasma levels of alanine aminotransferase (ALT) in C57BL/6 mice at 30 hours after intravenous injection of an anti-CD40 mAb (n=4) vs saline (n=3). (C) Heatmap displaying z-scaled levels of plasma cytokines in C57BL/6 mice at 7 (n=5), 16 (n=5), 24 (n=5) or 30 hours (n=5) after intravenous injection of an anti-CD40 mAb or saline (0 hour, n=2) (blue=low concentration, red=high concentration). (D) Outline of the multiplexed scRNA-seq experiment: C57BL/6 mice were intravenously injected with an anti-CD40 mAb or saline (0 hours). After saline injection (n=1) or 7 (n=1), 14 (n=1) and 22 hours (n=1) after anti-CD40 mAb, livers were digested into a single-cell suspension and enriched for leucocytes using CD45-coated magnetic beads. Cells were harvested, tagged with DNA-barcoded antibodies and pooled into a single scRNA-seq sample for sequencing. Data generated from this experiment are shown in the subsequent panels. (E) UMAP plot displaying cells colored by condition. (F) UMAP plot displaying cells colored by cell type. (G) UMAP plots separated by treatment conditions (anti-CD40 mAb treatment for 7, 14, or 22 hours or saline) with color saturation corresponding to cellular density. Below each UMAP plot are horizontal stacked bar charts displaying the proportions of different cell types, with the same code color as in Panel 1F. (H) Dot plot displaying the results of a differential gene expression (DEG) analysis between Kupffer cells from anti-CD40 mAb-treated (7 hours) and saline-treated mice. Points are plotted according to the log-transformed fold change (logFC) on the y-axis and the base mean on the x-axis and colored according to the -log(p value). (I) Plasma levels of ALT in LysMCre CD40$^{fl/fl}$ (n=5) and CD40$^{fl/fl}$ (wild-type, n=7) (left) or in Clec4fCre CD40$^{fl/fl}$ (n=8) and CD40$^{fl/fl}$ (n=6, wild-type) (right) mice at 30 hours after intravenous injection of anti-CD40 mAb. (J) Hierarchical clustering analysis of z-scaled levels of plasma cytokines in LysMCre CD40$^{fl/fl}$ (n=7) and CD40$^{fl/fl}$ (n=7) (left) or in Clec4fCre CD40$^{fl/fl}$ (n=5) and CD40$^{fl/fl}$ (n=8, wild-type) (right) mice treated with an anti-CD40 mAb (30 hours, green) or saline (purple) (blue=low concentration, red=high concentration). (K) The data in (B, I, J) are presented as the mean±SD Each dot (B, I, J) or row (C) represents one mouse. T-test (B, I, J); n.s.=not significant, **p≤0.01, ***p≤0.001. mAb, monoclonal antibody; UMAP, uniform manifold approximation and projection.

in Kupffer cells at 7 hours after anti-CD40 mAb treatment was consistent with a process in which initial Kupffer cell activation led to inflammatory monocyte recruitment (online supplemental figure 4A,B). At 22 hours, there was additional recruitment of S100a8[+] neutrophils. Across the whole process, we also observed a progressive shift in the endothelial cell population along an activation vector defined by progressive expression of the adhesion molecule Vcam1 (online supplemental figure 2A). The inflammatory activation of endothelial cells was consistent with the histopathological finding of extensive thromboses in the liver of the anti-CD40 mAb-treated mice.

The above described time course analysis suggested that Kupffer cell activation is the initial trigger of anti-CD40 mAb-induced liver disease. To evaluate the necessity of Kupffer cells as a driver of anti-CD40 mAb-induced immune toxicity in the liver, we studied two conditional CD40 knockout mouse strains. LysM-Cre CD40[flox/flox] mice have a deletion of CD40 in most macrophages throughout the body, while the deletion in Clec4f-Cre CD40[flox/flox] mice is restricted to Kupffer cells.[33] In both models, the increase in ALT expression observed following anti-CD40 mAb treatment was significantly decreased, and no necrosis was detected in these mice by histology (figure 1I). By contrast, hierarchical clustering analysis of plasma cytokine levels showed that the systemic inflammatory response was abolished in only the LysM-Cre mice and not in the Clec4f-Cre mice (figure 1J). These results demonstrate that, while lineage selective conditional knockout of CD40 in all macrophages abolished hepatic and nonhepatic inflammation, suppression of CD40 signaling in Clec4f^{+} Kupffer cells abrogates anti-CD40 mAb-induced necro-inflammatory liver disease with only minimal adverse effects on systemic innate immune activation.

Collectively, this suggested that Kupffer cells might be a preferable drug target for the selective suppression of anti-CD40 mAb-associated liver toxicity.

Ter119 targets RBCs for phagocytosis by liver macrophages

After identifying Kupffer cells as a potential drug target to suppress anti-CD40-induced liver toxicity, we next sought to selectively reprogram liver macrophages into an anti-inflammatory phenotype. Liver macrophages are the default erythrophagocytes under conditions of enhanced RBC turnover.[34] Furthermore, erythrophagocytosis followed by heme-activated NRF2 signaling transforms macrophages into an anti-inflammatory Hmox1^{high}Marco[high]MHCII[low] phenotype.[27] We therefore, evaluated strategies to induce a controlled erythrophagocytosis to selectively reprogram liver macrophages, providing a novel anti-inflammatory mode of action to overcome anti-CD40 mAb-mediated liver toxicity.

Ter119 is a rat mAb that recognizes a glycophorin-associated protein on mouse RBCs.[35] Using time-lapse fluorescence imaging, we demonstrated that Ter119 specifically induced the phagocytosis of pHrodo-labeled RBCs by mouse bone marrow (BM)-derived macrophages

(BMDMs) over time (figure 2A). To study whether Ter119 directs RBCs to be selectively phagocytosed by liver macrophages in vivo, we labeled mouse RBCs with carboxyfluorescein succinimidyl ester (CFSE), incubated the cells with Ter119, and tracked their clearance from the blood into the liver after intravenous injection by flow cytometry analysis (figure 2B). Staining of the blood with a fluorescent goat anti-rat secondary reagent (AF 555) allowed us to clearly distinguish the CFSE-labeled, Ter119-opsonized RBC population from RBCs only opsonized with Ter119 or labeled with CFSE (figure 2C). Within 1 hour, we noted a rapid decline of CFSE[+]Ter119^{+} RBCs from the peripheral blood, while nonopsonized RBCs remained in the circulation (figure 2D). Non-invasive fluorescence imaging combined with infrared fluorescent labeling of RBCs demonstrated that Ter119^{+} RBCs were specifically trapped in the liver. No fluorescence signal was observed in the heart, spleen, kidneys, or colon (figure 2E). Finally, by confocal microscopy and flow cytometry, we found that the fluorescence signal of CFSE-labeled, Ter119-opsonized RBCs was contained within the F4/80[+] liver macrophages (figure 2F–I). Collectively, these data suggest that Ter119 directs RBCs to be selectively phagocytosed by liver macrophages.

mTer119 induces the transformation of liver macrophages into erythrophagocytes

As a next step, we established a treatment protocol involving an initial high dose of Ter119 antibody followed by repeated low-dose injections, as delineated in figure 3A. This protocol allowed us to reach a hematopoietic steady state with stimulated erythropoiesis compensating for the accelerated RBC clearance by liver macrophages. To avoid adverse immunological reactions, such as anaphylaxis and the generation of neutralizing antibodies, it was critical for these studies involving repeated injections to use a recombinant murine IgG2 antibody (mTer119), which was derived from the original rat Ter119 clone.[30]

We first analyzed the effect of repeated mTer119 injections on liver macrophage counts. IF staining demonstrated a 40% increase in the number of F4/80[+] liver macrophages in mTer119-treated mice compared with control mice (figure 3B,C). This expansion of the liver macrophage population could be attributed to the recruitment of circulating monocytes using the Ms4a3[Cre]-Rosa[TdT] monocyte fate-mapper mouse strain. In this mouse granulocyte-monocyte progenitors, common monocyte progenitors,[36] and all their descendants are labeled by the fluorescent protein tdTomato. 24 hours after the last mTer119 injection, 40% of the CD45^{+}F480^{+}CD11b^{+} liver macrophages expressed tdTomato (online supplemental figure 5A,B), which was consistent with the overall 40% expansion of the macrophage pool. This expansion reflects the increased demand for erythrophagocytes, nevertheless we can not exclude that some Kupffer cells die after erythrophagocytosis and are subsequently replaced by recruited blood monocytes.
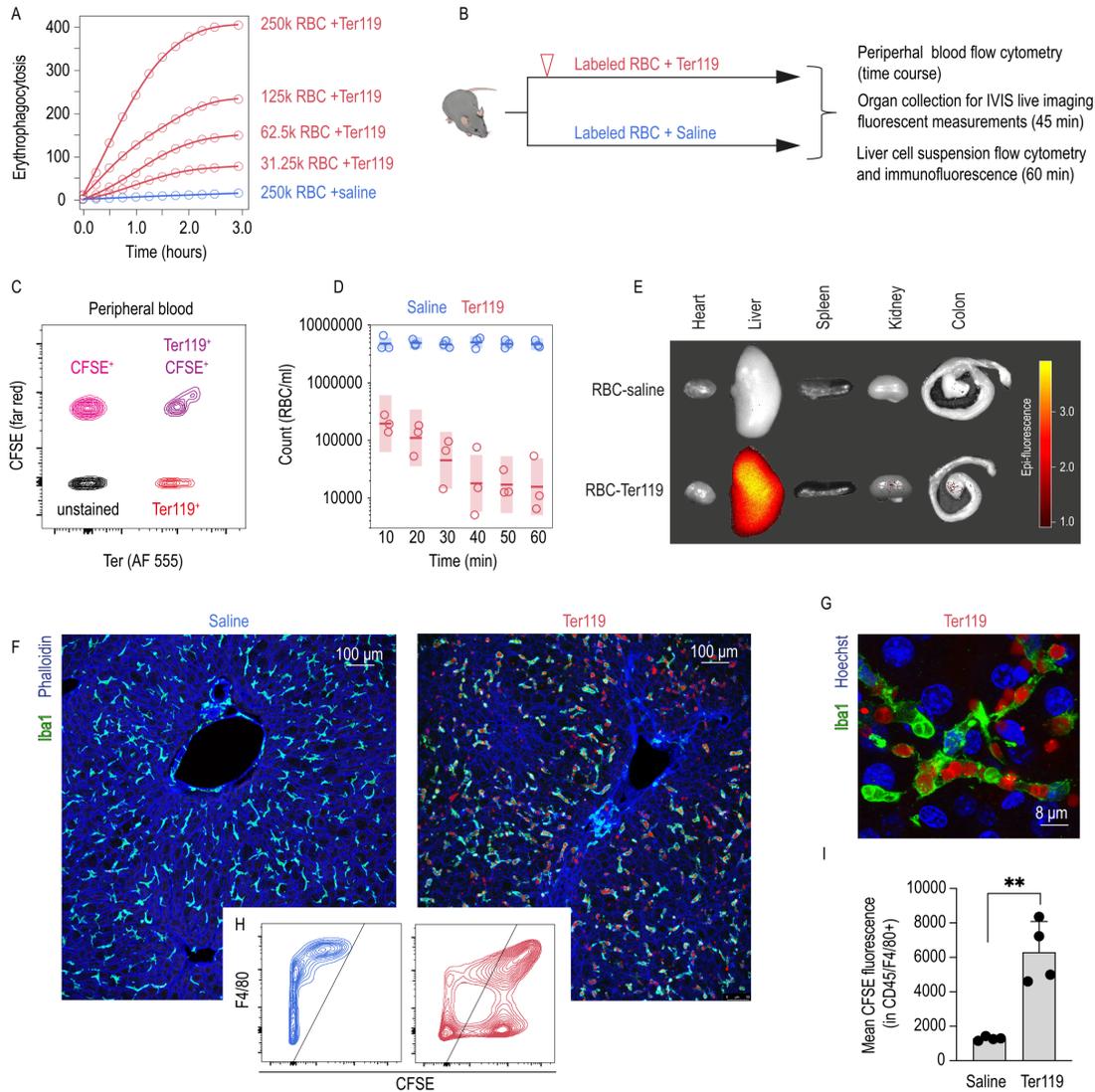
Figure 2 Ter119-opsonized RBCs are phagocytosed by liver macrophages. (A) BMDMs were exposed to different numbers of RBCs opsonized or not with the rat antibody Ter119 (400 µg/mL). Before exposition, the RBCs were labeled with red pHrodo. The cells were imaged every 15 min using a live-cell analyzer. The dot plot displays the mean fluorescence intensity of four replicates over time as a direct correlation to the number of phagocytosed erythrocytes. (B) Outline of the transfusion experiments: C57BL/6 mice were transfused with CFSE- or IVISense 680-labeled RBCs that were opsonized (Ter119+) or not (Ter119-) with the rat anti-mouse antibody Ter119 (667 µg/mL). Blood was collected every 10 min, and the clearance of the RBCs was analyzed by flow cytometry. After 45 min, the mice were sacrificed, and organs were collected for analysis with an IVIS Spectrum in vivo imaging system. Some animals were euthanized after 1 hour for flow cytometric analysis or liver histology of liver cell suspensions. (C) Untreated RBCs or in vitro rat Ter119-opsonized RBCs were labeled with CFSE (far red) or left unlabeled, and Ter119 opsonization was subsequently detected by staining the cells with an Alexa Fluor 555-conjugated goat anti-rat secondary antibody. The RBCs subjected to each treatment condition were pooled and evaluated by flow cytometry. (D) RBC clearance (number of CFSE-positive RBCs/mL of blood over time) after mouse transfusion as indicated in B. Blood was collected every 10 min and stained using an Alexa Fluor 555-coupled goat anti-rat secondary antibody to verify opsonization by the primary rat antibody Ter119. CFSE-positive RBCs were gated in each sample and counted to obtain the number per ml of blood. (E) Representative image of the far-red fluorescence of organs collected from mice transfused with IVIS sense 680-labeled Ter119+ or Ter119- (saline) RBCs 45 min after transfusion. Data are representative of three animals. (F) Representative immunofluorescence staining images of liver sections collected from mice transfused with CFSE-labeled Ter119+ or Ter119- RBCs (red) 1 hour after transfusion. The liver sections were stained with anti-Iba1 (green) and phalloidin (blue), and images were acquired with a confocal microscope using a 20× objective. (G) Representative immunofluorescence staining image of liver macrophages phagocytosing CFSE-labeled Ter119-opsonized RBCs (red). The image was acquired from a liver section stained with anti-Iba1 (green) and Hoechst (blue) under a confocal microscope using a 63× objective. (H) Flow cytometry contour plots of liver cell suspensions collected from mice transfused with CFSE-labeled Ter119+ or Ter119- RBCs 1 hour after transfusion. Cells were stained for F4/80 and gated from live CD45+ cells. (I) Cumulative data for the mean CFSE fluorescence intensity of CD45+F4/80+ cells in liver cell suspensions from mice transfused as described in H (n=4). (J) The data in I are presented as the mean±SD. Each dot represents one mouse (D, I) or one well (A). t test (I); **p≤0.01. BMDMs, bone marrow-derived macrophages; CFSE, carboxyfluorescein succinimidyl ester; RBCs, red blood cells.
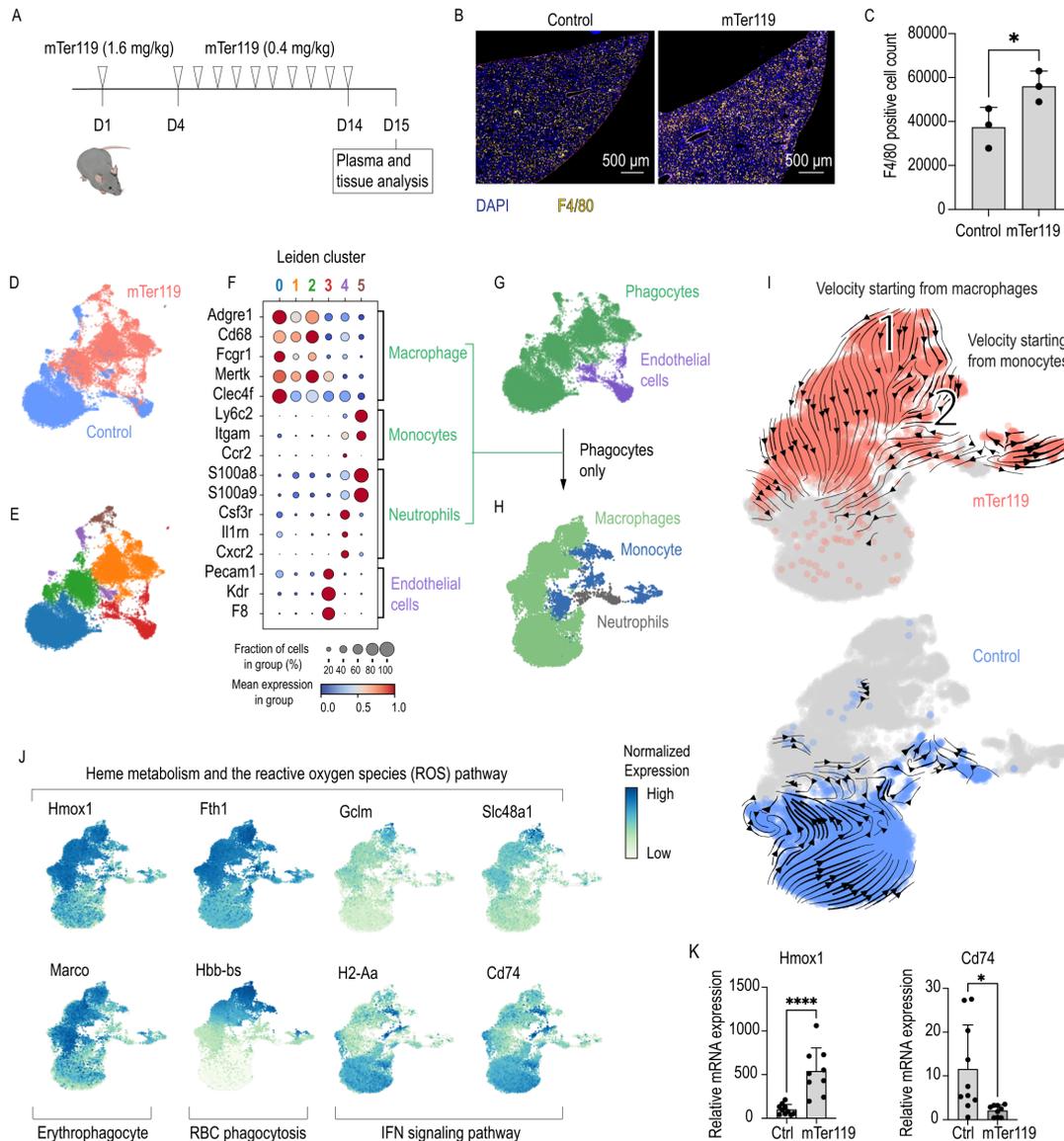
Figure 3 Chronic mTer119 antibody treatment transforms liver macrophages into erythrophagocytes. (A) Outline of the mTer119 treatment protocol: C57BL/6 mice were treated subcutaneously with a loading dose of the murine Ter119 (mTer119) antibody (1.4 mg/kg). After 4 days, a low dose (0.4 mg/kg) of the antibody was given on a daily basis for 10 days. The animals were sacrificed 24 hours after the last injection for analysis. As a control, saline or isotype control was injected with the same volume, concentration and frequency. (B) Representative immunofluorescence staining images of paraffin-embedded liver sections from C57BL/6 mice subjected to mTer119 treatment. The liver sections were stained with anti-F4/80 (yellow) and DAPI (blue), and the images were acquired using a Zeiss Axio scan. (C) Morphometric quantification of F4/80$^+$ macrophage counts based on stained whole-liver sections from C57BL/6 mice subjected to mTer119 (n=3) or saline treatment (n=3). (D) UMAP plot of pooled scRNA-seq data from two sequencing experiments performed with liver cell suspensions from mTer119- (n=1) and saline-treated (n=1) mice. Before sequencing, the liver cells were enriched for macrophages using anti-F4/80 and anti-CD11b-coated magnetic beads. The enriched cell suspensions were then processed for scRNA-seq. Cells are colored by treatment (mTer119 or saline). (E) UMAP plot of cells colored by clusters as computed by the Leiden unsupervised clustering algorithm. (F) Dot plot displaying the scaled expression of canonical marker genes for each cell type and the proportion of cells in each cluster expressing those genes. (G) UMAP plot displaying cells colored by cell type. Macrophages, monocytes, and neutrophils were regrouped and displayed as phagocytes. (H) All cells marked as phagocytes in G were pooled into a new dataset and dimension reduction was calculated. UMAP plot displaying cells colored by cell type. (I) UMAP plots with cells colored by sample. RNA velocity vectors are superimposed onto the UMAP plots with arrows indicating the velocity direction and magnitude (arrow length). Velocities were calculated for each sample separately, only including the phagocyte populations (top: mTer119, bottom: saline). (J) UMAP plots with cells colored according to their expression of key genes associated with the erythrophagocytic phenotype (yellow=low expression, blue=high expression). (G) Hmox1 and Cd74 mRNA expression measured by RT-qPCR of liver macrophage isolated using anti-F4/80 coated magnetic beads from animals treated with isotype control (n=10) or mTer119 (n=9). (H) The data in C and K are presented as the mean±SD Each dot represents one mouse. T-test (C, K); *p≤0.05, ****p≤0.0001. RBC, red blood cell; scRNA-seq, single-cell RNA-sequencing; UMAP, uniform manifold approximation and projection.

To study the phenotype of liver macrophages after mTer119 treatment, we performed a scRNA-seq study of liver cells that were enriched for macrophages by combined F4/80 and CD11b magnetic bead capture. In total, 9480 cells were analyzed from a mTer119-treated mouse, and 9611 cells were analyzed from a vehicle-treated mouse (figure 3D). By matching the gene expression of each cluster with canonical marker genes, we classified the cell clusters as macrophages, monocytes, neutrophils, and endothelial cells (figure 3E,F, online supplemental figure 6A,B). After regrouping all phagocytic cells, we recalculated dimension reduction and cell type assignment (figure 3G,H). We could observe a stark separation with little overlap of the phagocytes in the two conditions (figure 3I) indicating a pronounced effect of mTer119 on their transcriptional phenotype. We next performed a differential gene expression analysis between the macrophages of the antibody-treated mouse versus the vehicle-treated mouse before pathway enrichment analysis by GSEA (online supplemental figure 6C). Liver macrophages from the mTer119-treated mouse strongly increased expression of genes involved in heme metabolism and the reactive oxygen species pathway (Hmox1, Fth1, Gclm, Slc48a1) and the erythrophagocyte marker gene Marco,[27] while genes linked to IFN signaling pathways and the inflammatory response (H2-Aa and Cd74) were suppressed (online supplemental figure 6D,E, examples highlighted in figure 3J). In the mTer119-treated mouse phagocytes, RNA velocity analysis revealed the direction of differentiation starting from macrophages (1) and monocytes (2). In both cases, the initial cell populations have a high Hbb-bs mRNA content, suggesting that macrophages undergo a differentiation process driven by phagocytosis of erythrocytes (figure 3I,J).

We confirmed the scRNA-seq data in a separate experiment by analyzing Hmox1 and Cd74 mRNA of liver macrophages that were isolated using anti-F4/80 antibody-coated Dynabeads from mTer119-treated mice and mice treated with an isotype-matched control antibody. We identified the same erythrophagocytic signature with increased expression of Hmox1 and suppressed Cd74 in the mTer119-treated animals (figure 3K). As further validation, we detected a strong increase of HMOX1 in liver macrophages of mTer119-treated mice compared with control animals by fluorescence immunohistochemistry. On mTer119-treatment, the fraction of F4/80$^+$/HMOX1$^+$ double positive macrophages increased from 6.9% to 67.8% (online supplemental figure 5C,D).

Collectively, these data suggest that mTer119 treatment induced extensive phenotypic transformation of the liver macrophages of mixed ontogeny, supporting the generation of a homogenous population of Hmox1^{high}Marco^{high}MHCII^{low} erythrophagocytes.

mTer119 prevents liver inflammatory toxicity induced by high-dose anti-CD40 mAb administration

To determine whether the mTer119-induced transformation of liver macrophages into erythrophagocytes could protect against anti-CD40 mAb-triggered liver disease, we challenged mTer119-treated mice with an anti-CD40 mAb 24 hours after the last mTer119 injection and analyzed the inflammatory response and liver toxicity 30 hours later (figure 4A). mTer119 treatment prevented the generation of morphological evidence of liver necrosis (figure 4B,C) and the increase of ALT plasma levels (figure 4D). However, anti-CD40 mAb-induced plasma cytokine levels remained high despite mTer119 treatment, consistent with a liver-selective mode of action (figure 4E). Ter119 treatment did also not reduce anti-CD40 mAb-induced colitis, as denoted by similar increases in colon crypt length and the disappearance of goblet cells (figure 4F,G) in both mTer119-treated mice and control mice subjected to anti-CD40 mAb.

Collectively, these experiments suggest that mTer119-induced erythrophagocytic transformation exhibits liver-specific anti-inflammatory organ tropism.

mTer119 suppresses selectively anti-CD40 mAb-induced hepatic macrophage inflammation

To further assess whether the mTer119-induced anti-inflammatory effect is liver-specific, we analyzed the CD40 ligation-induced cytokine mRNA expression of F4/80$^+$ macrophages isolated from the liver, colon, or peritoneal cavity of anti-CD40 mAb versus saline-treated mice. We also compared the anti-inflammatory activity of mTer119 with the one issued by the TNF blocker etanercept, which is a non-liver specific anti-inflammatory and immunosuppressive drug (figure 4H). Figure 4I provides a visual representation of the early mRNA expression levels of the inflammation markers Cxcl9, Cxcl10, and Il12b in colon and liver macrophages 16 hours after anti-CD40 mAb treatment quantified by RT-qPCR. An unsupervised clustering analysis allowed us to segregate the macrophages into two main clusters, which were defined as 'inflamed' and 'noninflamed', based on the cytokine expression of saline-treated (control) and anti-CD40 mAb-treated animals. This clustering could then be used to classify the macrophage samples from mTer119 plus anti-CD40 mAb-treated animals in a cross table. All colon macrophage samples from the mTer119 plus anti-CD40 mAb group were classified as inflamed, suggesting that mTer119 treatment did not attenuate anti-CD40 mAb-triggered inflammation in colon macrophages. By contrast, all liver macrophage samples from the mTer119 plus anti-CD40 mAb animals were classified as noninflamed, confirming the robust and specific anti-inflammatory effect of mTer119 treatment on the liver (figure 4J). In contrast to the liver-specific anti-inflammatory activity of mTer119, pretreatment of mice with etanercept (eta) before anti-CD40 mAb treatment profoundly suppressed the cytokine responses in both organs (figure 4K,L). Similar results were observed in a separate study analyzing the response
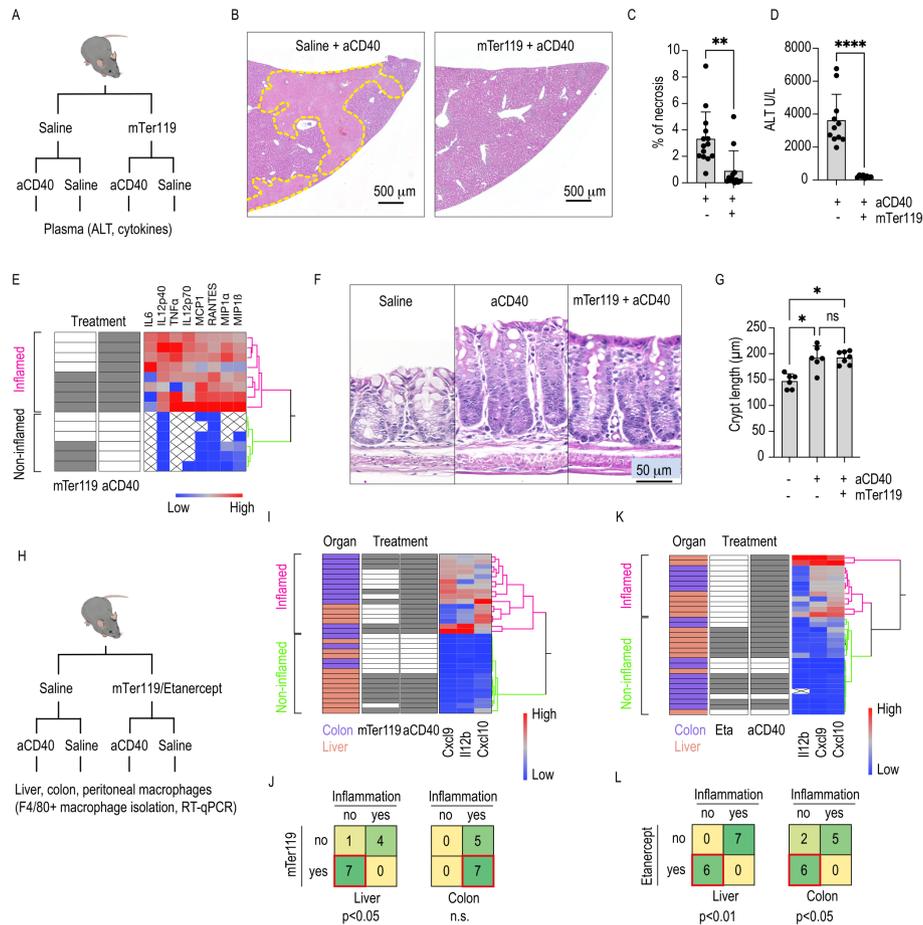
Figure 4 Chronic mTer119 treatment protects against liver toxicity induced by anti-CD40 mAb treatment. (A) Experimental design for anti-CD40 mAb challenge: C57BL/6 mice were first subjected to mTer119 treatment (1.4 mg/kg, followed by 0.4 mg/kg daily) before challenge with anti-CD40 mAb (20 mg/kg) 24 hours after the last dose of mTer119. The mice were sacrificed 16 or 30 hours later for cytokine or plasma transaminase measurements, respectively. (B) Representative images of liver sections stained with H&E from a C57BL/6 mouse subjected to mTer119 (n=12) or saline treatment (n=14) and challenged with an anti-CD40 mAb. (C) Morphometric quantification of the necrotic area (percentage of the total liver area) of mice treated as described in A (mTer119 n=12, saline n=14). (D) Plasma ALT levels measured in C57BL/6 mice subjected to mTer119 (n=8) or saline treatment (n=11) and challenged with an anti-CD40 mAb. (E) Heatmap showing unsupervised hierarchical clustering of plasma cytokine levels in C57BL/6 mice subjected to mTer119 (n=7) or saline treatment (n=7) and challenged with an anti-CD40 mAb (n=8, blue=low concentration, red=high concentration) (gray mark=presence of treatment, white=absence of treatment). (F) Representative images of crypts in colon sections stained with H&E from a C57BL/6 mouse subjected to mTer119 antibody treatment or saline treatment and challenged with or without an anti-CD40 mAb. (G) Average crypt length (μm) calculated from 20 measurements of colon sections from C57BL/6 mice subjected to mTer119 (n=7) or saline treatment (n=6) and challenged with or without an anti-CD40 mAb. (H) Experimental design for anti-CD40 mAb challenge with macrophage isolation: C57BL/6 mice were first subjected to mTer119 treatment before challenge with anti-CD40 mAb 24 hours after the last dose of mTer119. The mice were sacrificed 16 hours later and underwent peritoneal lavage as well as liver and colon harvesting and digestion. Single-cell suspensions from the liver, colon and peritoneal cavity were enriched for macrophages using F4/80-coated Dynabeads, and macrophage gene expression was analyzed by RT-qPCR. (I) Heatmap showing unsupervised hierarchical clustering analysis of Cxcl9, Cxcl10 and Il12b gene expression in liver (orange) or colon (purple) macrophages in C57BL/6 mice subjected to mTer119 antibody treatment or saline treatment and challenged with or without an anti-CD40 mAb. Organs were digested into single-cell suspensions, macrophages were isolated using anti-F4/80-coated magnetic beads, and gene expression was measured by RT-qPCR (blue=low gene expression, red=high gene expression). The clustering analysis classified animals into inflamed and noninflamed groups (gray mark=presence of treatment, white=absence of treatment). (J) Contingency tables (mTer119 treatment × inflammation) of the classified animals separated by organ; data were analyzed with Fisher's exact test. (K) Heatmap showing unsupervised hierarchical clustering analysis of Cxcl9, Cxcl10 and Il12b gene expression in liver (orange) or colon (purple) macrophages in C57BL/6 mice subjected to etanercept (eta) treatment (two intraperitoneal (i.p.) injections of 100 mg/kg on days −3 and −1) or saline treatment and challenged with or without an anti-CD40 mAb. The clustering analysis classified animals into inflamed and noninflamed groups (gray mark=presence of treatment, white=absence of treatment). (H) Contingency tables (etanercept treatment x inflammation) of the classified animals separated by organ; data were analyzed with Fisher's exact test. The data in C, D, and G are presented as the mean±SD. Each dot (C, D, G) or row (E, I, K) represents one mouse. T-test (C, D), ANOVA (G), Fisher's exact test (J, L); n.s.=not significant, *p≤0.05, **p≤0.01, ****p≤0.0001. ANOVA, analysis of variance; mAb, monoclonal antibody.

of peritoneal macrophages; mTer119 did not change the inflammatory outcome of anti-CD40 treatment, but the inflammatory cytokine response induced by anti-CD40 mAb treatment was attenuated by etanercept (online supplemental figure 7A,B).

Collectively, these experiments demonstrated that mTer119 selectively suppressed macrophage inflammation in the liver, leaving the inflammatory responses of macrophages in the colon and peritoneum unaffected. This organotropic anti-inflammatory function diverged from the function of etanercept, which non-selectively impaired inflammation in the liver, colon and peritoneum.

mTer119 does not suppress systemic immunity or the antitumor activity of anti-CD40 mAbs

After establishing the organotropic nature of the effect of mTer119 on anti-CD40 mAb-induced inflammatory toxicity, we aimed to determine whether mTer119 has anti-inflammatory or immunosuppressive effects in generic models of systemic inflammation.

First, we investigated the effect of mTer119 on systemic inflammation after the injection of lipopolysaccharide (LPS) or an agonist anti-CD3 antibody by measuring plasma cytokines 4 hours after LPS injection and 3 hours after anti-CD3 antibody injection. In both experiments, hierarchical clustering analysis confirmed that mTer119 treatment had no systemic anti-inflammatory effect (figure 5A,B, online supplemental figure 8).

Second, we evaluated antigen-specific CD8$^+$ and CD4$^+$ T-cell responses using OT-1 and OT-2 recombinant T cell receptor mouse models. The T cells of these mice recognize OVA protein presented in the context of MHC class I or II, respectively. CFSE-labeled CD8$^+$ and CD4$^+$ T cells from OT-1 and OT-2 CD45.1 mice, respectively, were transferred into mTer119- or saline-treated C57BL/6 CD45.2 mice by intravenous injection. The proliferation of CD45.1$^+$ T cells in the draining lymph nodes was measured 3 days after subcutaneous administration of ovalbumin with or without anti-CD40 mAb treatment. The administration of ovalbumin combined with anti-CD40 mAb increased the proliferation of antigen-specific CD45.1$^+$CD8$^+$ or CD4$^+$ T cells in the lymph nodes compared with that on the administration of ovalbumin alone, indicating that the anti-CD40 mAb is an excellent enhancer of antigen-specific T-cell stimulation in this model. mTer119 treatment did not attenuate this response (figure 5C, online supplemental figure 7C,D).

Finally, we assessed whether mTer119 treatment affects the antitumor effect of anti-CD40 mAb therapy using a mouse MC38 colon adenocarcinoma tumor. We subcutaneously injected tumor cells into saline- or mTer119-treated mice (day 1) and then administered two injections of anti-CD40 mAb on days 7 and 9; the tumor volume was measured at regular intervals up to day 14. We found that anti-CD40 mAb treatment significantly diminished cancer cell growth and that mTer119 did not abolish this beneficial treatment effect (figure 5D).

Collectively, these results suggest that the targeted erythrophagocytic transformation of liver macrophages induced by mTer119 treatment does not suppress innate or adaptive immune responses or antitumor immunity outside the liver.

DISCUSSION

Immune-mediated liver toxicity has been recognized as a dose-limiting adverse effect of agonistic anti-CD40 mAbs.[13] To decipher the mechanism of liver toxicity and rationally design a strategy to abrogate this off-target effect without blunting the antitumor efficacy, we performed a time-resolved scRNA-seq study, which delineated a sequence of initial Kupffer cell activation, followed by monocyte recruitment and the subsequent accumulation of neutrophilic granulocytes. In parallel, we observed progressive inflammatory endothelial cell activation consistent with widespread thrombotic liver ischemia. Subsequent experiments with CD40 conditional knockout mice revealed the decisive triggering function of Kupffer cells in this cascade. The precise pathophysiological framework derived from these studies suggested that a selective anti-inflammatory reprogramming strategy targeting Kupffer cells could disconnect the hepatic and extrahepatic immunostimulatory activities of high-dose anti-CD40 mAb treatment protocols. In the next step, we provide evidence that the tissue-specific function of liver macrophages to clear RBCs from the blood can be exploited to selectively induce a heme-driven anti-inflammatory pathway. Targeting host RBCs with a recombinant mAb protected mice against liver toxicity associated with high-dose administration of agonistic anti-CD40 mAbs. The same treatment protocol did not attenuate anti-CD40 mAb-induced systemic inflammation, peripheral antigen-specific immunity enhancement, or tumor control, suggesting that this approach uncouples the proinflammatory and anti-inflammatory macrophage signaling pathways of hepatic and extrahepatic macrophage populations.

Our therapeutic reprogramming strategy takes advantage of the unique function of resident liver macrophages to trap and phagocytose antibody-marked RBCs from the blood during hemolytic stress.[34 37] Consistent with this model, we have presented the results from a number of experiments demonstrating that Ter119-IgG2-opsonized RBCs localized selectively to liver macrophages shortly after infusion and that repeated low-dose mTer119 administration induced a phenotypic switch in liver macrophages into anti-inflammatory erythrophagocytes, providing protection against high-dose anti-CD40 mAb-induced liver toxicity. Our scRNA-seq and fate mapping studies revealed that the phenotypically homogenous erythrophagocytes had a mixed ontogeny of phenotype-transformed Kupffer cells and peripheral blood monocytes most likely recruited via Ccl2-Ccr2 signaling. This is consistent with the previous observation that administration of a single large dose of the Ter119 antibody leads
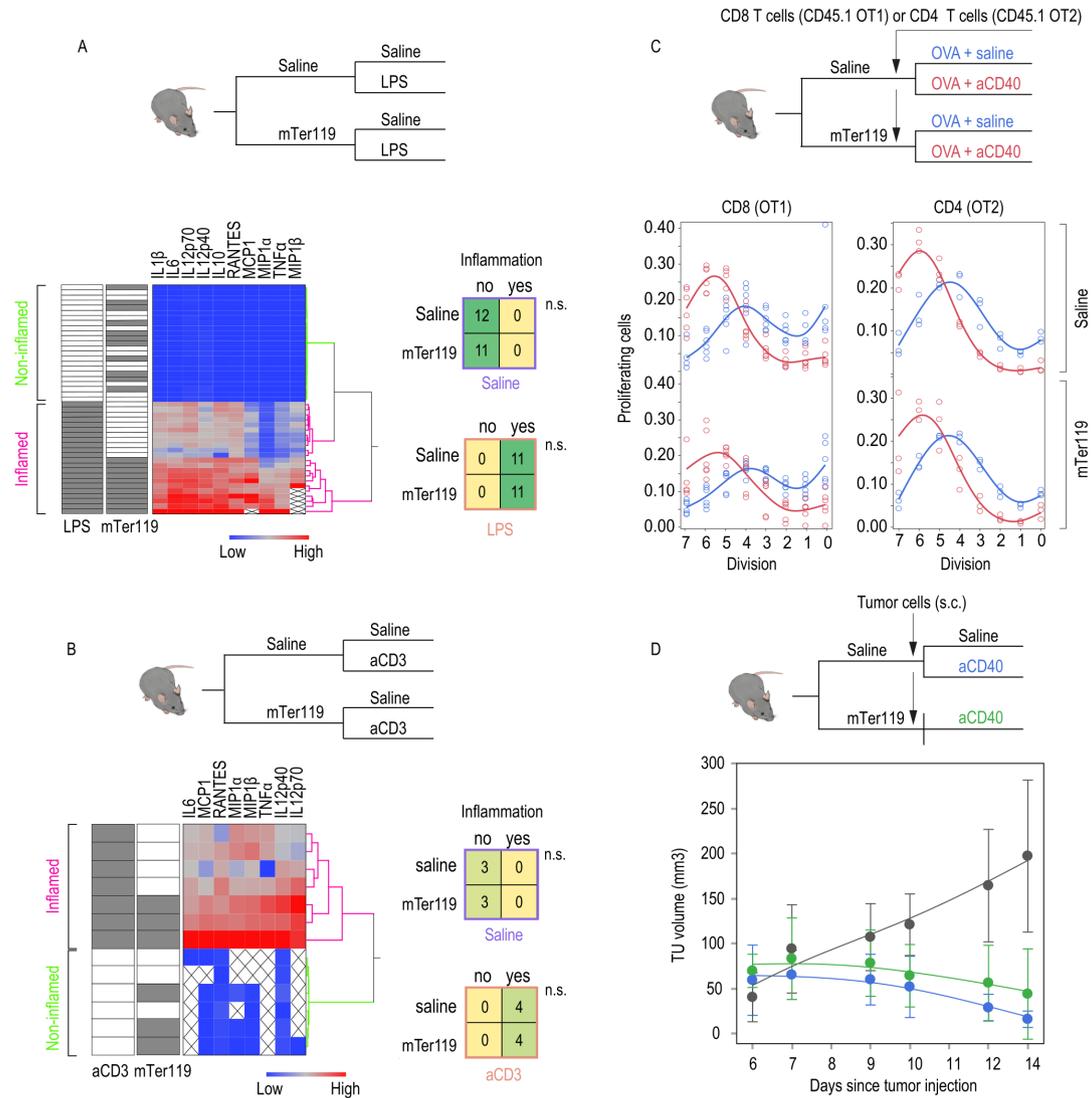
Figure 5 Anti-CD40 mAb-mediated systemic inflammation and antitumor activity are preserved with mTer119 treatment. (A) Experimental design of the LPS experiment: C57BL/6 mice were chronically treated with the antibody mTer119 or saline and injected i.p. with LPS (6 mg/kg). Blood was sampled before and 4 hours after the LPS injection to measure cytokine levels. Bottom left: Heatmap showing unsupervised hierarchical clustering analysis of plasma cytokine levels (blue=low concentration, red=high concentration). The clustering analysis classified animals into inflamed and noninflamed groups. Bottom right: Contingency tables summarizing the effects of mTer119 on inflammation status in saline- and LPS-treated animals; data were analyzed with Fisher's exact test with a significance threshold of $p \leq 0.05$ (n.s.=not significant). (B) Experimental design of the agonistic anti-CD3 antibody experiment: C57BL/6 mice were chronically treated with the antibody mTer119 or saline and injected intravenous with an anti-CD3 antibody (100 µg). Four hours later, the animals were sacrificed, and blood was collected for proinflammatory cytokine measurement. Bottom left: Heatmap showing unsupervised hierarchical clustering analysis of plasma cytokines (blue=low concentration, red=high concentration). Bottom right: Contingency tables summarizing the effects of mTer119 on the inflammation status in saline- and anti-CD3-treated animals; data were analyzed with Fisher's exact test with a significance threshold of $p \leq 0.05$ (n.s.=not significant). (C) Schematic representation of the adoptive transfer experiment. CD8^{+} and CD4^{+} T cells were isolated from the spleen of CD45.1 x OT-1 or CD45.1 x OT-2 mice, labeled with CFSE and injected intravenous into mTer119 or saline-treated mice. Two hours later, the mice were subcutaneously immunized with the ovalbumin (OVA) protein mixed with or without an anti-CD40 mAb. Three days later, the draining lymph nodes were collected, and the proliferation of transferred T cells was assessed by evaluating the degree of CFSE dilution by flow cytometry. Bottom: Cumulative data showing the proportion of proliferating cells within each division for each condition. The number of divisions was assessed by measuring the dilution of the CFSE signal. (D) Experimental design for mTer119+anti-CD40 mAb treatment of tumor-bearing mice: C57BL/6J mice were treated with mTer119 (1.4 mg/kg, followed by 0.4 mg/kg daily) or saline for 7 days before s.c. injection of MC38 tumor cells into the flanks. The tumors were left to grow for seven more days while continuing daily mTer119 treatment before intravenous injection of an anti-CD40 mAb (20 mg/kg) for a first time, followed by a second intravenous injection on day 9. Tumor volume was measured 1 day before anti-CD40 mAb treatment (day 6) and every other day until the end of the experiment on day 15. Bottom: Line plot displaying MC38 tumor volume over time (days after tumor injection). Each dot represents the mean of five animals±95% CI (n=5). Each dot (C) or row (A, B) represents one mouse. CFSE, carboxyfluorescein succinimidyl ester; LPS, lipopolysaccharide.

to rapid secretion of the monocyte-attracting chemokine CCL2, monocytosis in the blood, and subsequent recruitment of monocytes to the liver macrophage niche.[30] This hematopoietic feedback loop rapidly expands erythrophagocyte capacity in the liver during hemolytic stress.

Induced erythrophagocytosis exploits a unique mode of action by delivering large doses of the endogenous metabolite heme into macrophages, where it evokes a pronounced anti-inflammatory effect via oxidative signaling and NRF2 activation.[27] The liver-selective organ tropism provided by our erythrophagocytosis-based macrophage reprogramming strategy is essential. Heme could act as an oxidative toxin if hemolysis would be induced in a less specific way,[31 38] and widespread activation of heme-NRF2 signaling in the hematopoietic compartment causes severe dysfunction in the myeloid lineage,[39] resulting in deficient dendritic cell generation, impaired antigen presentation, and macrophage dysfunction.[40] This has been observed in mouse models of sickle cell anemia and spherocytosis, both of which display intravascular hemolysis with systemic heme exposure and immunosuppression.[40] Additionally, administration of a single large dose of Ter119 was shown to induce a transient anti-inflammatory state in mice via an unresolved mechanism.[30] In light of these observations, we performed a thorough search for extrahepatic off-target effects of our treatment protocol. We not only investigated anti-CD40 mAb-induced systemic inflammation and antigen-specific immune augmentation, but also explored more generic inflammatory models induced by LPS or agonistic anti-CD3 antibody injection. None of these studies identified a signal of systemic immunosuppression by mTer119, supporting its liver specific activity. This might be a significant advantage over non-liver-selective macrophage targeting strategies (eg, by using CSF1 blocking agents), because tumoricidal macrophage activation induced by anti-CD40 antibodies seems to support therapeutic efficacy.[2 41]

While our model aims at selectively attenuating anti-CD40 antibody effects in the liver, alternative approaches aim to prevent liver toxicity by selectively enhancing CD40 activity in the tumor or subsets of immune cells driving antitumor effects. Such approaches have been expedited by the innovative design of bispecific antibodies targeting tumor-associated antigens or dendritic cell surface markers, in addition to CD40, or by selective delivery of CD40 agonists into the tumor tissue.[42–48]

The practical translation of our RBC-based macrophage reprogramming approach has to be defined in future preclinical studies focused on tolerability, safety, and efficacy. A significant parameter to be defined is how to reach a level of erythrophagocytosis in the liver sufficient to achieve consistent liver protection while avoiding severe hemolytic anemia. Potential strategies may include repeat low-dose antibody dosing, erythropoietic growth-factor support, or prophylactic retransfusion of antibody-coated autologous RBCs in patients undergoing anti-CD40 therapy. Ultimately, the clinical acceptance of any of these approaches will be determined by the magnitude by which clinical efficacy could be enhanced by applying high-dose antibody protocols with absent or significantly reduced liver toxicity.

Collectively, our experiments establish the fundamental concept that organ-specific reprogramming of macrophage phenotypes can fine-tune the response to systemic immunotherapy, uncoupling undesirable irAEs from antitumor activity. Such a prophylactic 'conditioning' strategy could significantly expand the safety margin of treatment protocols to allow use of higher and more effective doses of immunostimulatory antibodies. Beyond treating irAEs, selective anti-inflammatory reprogramming of liver macrophages could be a promising strategy to therapeutically approach a broader spectrum of inflammatory liver diseases, such as nonalcoholic fatty liver disease, alcoholic liver disease, and viral hepatitis.

ORCID iDs
Nadja Schulthess-Lutz http://orcid.org/0000-0002-2918-6262
Florence Vallelian http://orcid.org/0000-0001-9659-8278

REFERENCES
1 Nowak AK, Robinson BWS, Lake RA. Synergy between chemotherapy and immunotherapy in the treatment of established murine solid tumors. *Cancer Res* 2003;63:4490–6.

2 Beatty GL, Chiorean EG, Fishman MP, *et al*. CD40 agonists alter tumor stroma and show efficacy against pancreatic carcinoma in mice and humans. *Science* 2011;331:1612–6.

3 Byrne KT, Vonderheide RH. CD40 stimulation obviates innate sensors and drives T cell immunity in cancer. *Cell Rep* 2016;15:2719–32.

4 Vonderheide RH. CD40 agonist antibodies in cancer immunotherapy. *Annu Rev Med* 2020;71:47–58.

5 French RR, Chan HT, Tutt AL, *et al*. CD40 antibody evokes a cytotoxic T-cell response that eradicates lymphoma and bypasses T-cell help. *Nat Med* 1999;5:548–53.

6 Diehl L, den Boer AT, Schoenberger SP, *et al*. Cd40 activation in vivo overcomes peptide-induced peripheral cytotoxic T-lymphocyte tolerance and augments anti-tumor vaccine efficacy. *Nat Med* 1999;5:774–9.

7 Sotomayor EM, Borrello I, Tubb E, *et al*. Conversion of tumor-specific CD4+ T-cell tolerance to T-cell priming through in vivo ligation of CD40. *Nat Med* 1999;5:780–7.

8 Vonderheide RH, Glennie MJ. Agonistic CD40 antibodies and cancer therapy. *Clin Cancer Res* 2013;19:1035–43.

9 Schoenberger SP, Toes RE, van der Voort EI, *et al*. T-cell help for cytotoxic T lymphocytes is mediated by CD40-CD40L interactions. *Nature* 1998;393:480–3.

10 Buhtoiarov IN, Lum H, Berke G, *et al*. CD40 ligation activates murine macrophages via an IFN-gamma-dependent mechanism resulting in tumor cell destruction in vitro. *J Immunol* 2005;174:6013–22.

11 Long KB, Gladney WL, Tooker GM, *et al*. IFNγ and CCL2 cooperate to redirect tumor-infiltrating monocytes to degrade fibrosis and enhance chemotherapy efficacy in pancreatic carcinoma. *Cancer Discov* 2016;6:400–13.

12 Ingoglia G, Yalamanoglu A, Pfefferlé M, *et al*. Line-selective macrophage activation with an anti-CD40 antibody drives a hemophagocytic syndrome in mice. *Blood Adv* 2020;4:2751–61.

13 Siwicki M, Gort-Freitas NA, Messemaker M, *et al*. Resident Kupffer cells and neutrophils drive liver toxicity in cancer immunotherapy. *Sci Immunol* 2021;6. doi:10.1126/sciimmunol.abi7083. [Epub ahead of print: 02 Jul 2021].

14 Byrne KT, Leisenring NH, Bajor DL, *et al*. CSF-1R-Dependent lethal hepatotoxicity when agonistic CD40 antibody is given before but not after chemotherapy. *J Immunol* 2016;197:179–87.

15 Bonnans C, Thomas G, He W, *et al*. CD40 agonist-induced IL-12p40 potentiates hepatotoxicity. *J Immunother Cancer* 2020;8:e000624.

16 Machiels J-P, Gomez-Roca C, Michot J-M, *et al*. Phase Ib study of anti-CSF-1R antibody emactuzumab in combination with CD40 agonist selicrelumab in advanced solid tumor patients. *J Immunother Cancer* 2020;8. doi:10.1136/jitc-2020-001153. [Epub ahead of print: Available from].

17 Vonderheide RH, Flaherty KT, Khalil M, *et al*. Clinical activity and immune modulation in cancer patients treated with CP-870,893, a novel CD40 agonist monoclonal antibody. *J Clin Oncol* 2007;25:876–83.

18 Beatty GL, Li Y, Long KB. Cancer immunotherapy: activating innate and adaptive immunity through CD40 agonists. *Expert Rev Anticancer Ther* 2017;17:175–86.

19 De Martin E, Michot J-M, Rosmorduc O, *et al*. Liver toxicity as a limiting factor to the increasing use of immune checkpoint inhibitors. *JHEP Reports* 2020;2:100170.

20 Johnson DH, Zobniw CM, Trinh VA, *et al*. Infliximab associated with faster symptom resolution compared with corticosteroids alone for the management of immune-related enterocolitis. *J Immunother Cancer* 2018;6:103.

21 Badran YR, Cohen JV, Brastianos PK, *et al*. Concurrent therapy with immune checkpoint inhibitors and TNFα blockade in patients with gastrointestinal immune-related adverse events. *J Immunother Cancer* 2019;7:226.

22 Chen AY, Wolchok JD, Bass AR. TNF in the era of immune checkpoint inhibitors: friend or foe? *Nat Rev Rheumatol* 2021;17:213–23.

23 Suijkerbuijk KPM, Verheijden RJ. TNF inhibition for immune checkpoint inhibitor-induced irAEs: the jury is still out. *Nat Rev Rheumatol* 2021;17:505. doi:10.1038/s41584-021-00640-z

24 Jacoberger-Foissac C, Blake SJ, Liu J, *et al*. Concomitant or delayed anti-TNF differentially impact on immune-related adverse events and antitumor efficacy after anti-CD40 therapy. *J Immunother Cancer* 2020;8. doi:10.1136/jitc-2020-001687. [Epub ahead of print: Available from].

25 Stone ML, Lee J, Herrera VM, *et al*. TNF blockade uncouples toxicity from antitumor efficacy induced with CD40 chemoimmunotherapy. *JCI Insight* 2021;6. doi:10.1172/jci.insight.146314. [Epub ahead of print: 22 Jul 2021].

26 Vallelian F, Buehler PW, Schaer DJ. Hemolysis, free hemoglobin toxicity, and scavenger protein therapeutics. *Blood* 2022;140:1844 doi:10.1182/blood.2022015596

27 Pfefferlé M, Ingoglia G, Schaer CA, *et al*. Hemolysis transforms liver macrophages into antiinflammatory erythrophagocytes. *J Clin Invest* 2020;130:5576–90. doi:10.1172/JCI137282

28 Pfefferlé M, Ingoglia G, Schaer CA, *et al*. Acute hemolysis and heme suppress anti-CD40 antibody-induced Necro-Inflammatory liver disease. *Front Immunol* 2021;12:680855.

29 Humar R, Schaer DJ, Vallelian F. Erythrophagocytes in hemolytic anemia, wound healing, and cancer. *Trends Mol Med* 2022;28:915 doi:10.1016/j.molmed.2022.08.005

30 Crow AR, Kapur R, Koernig S, *et al*. Treating murine inflammatory diseases with an anti-erythrocyte antibody. *Sci Transl Med* 2019;11. doi:10.1126/scitranslmed.aau8217. [Epub ahead of print: 21 Aug 2019].

31 Schaer CA, Deuel JW, Bittermann AG, *et al*. Mechanisms of haptoglobin protection against hemoglobin peroxidation triggered endothelial damage. *Cell Death Differ* 2013;20:1569–79.

32 Pfefferlé M. Data from: targeted erythrophagocyte reprogramming of Kupffer cells halts cancer immunotherapy associated liver toxicity, 2022. NCBI Gene expression omnibus [dataset]. Available: https://www.ncbi.nlm.nih.gov/geo/query/acc.cgi?acc=GSE202918

33 Jiang Y, Tang Y, Hoover C, *et al*. Kupffer cell receptor CLEC4F is important for the destruction of desialylated platelets in mice. *Cell Death Differ* 2021;28:3009–21.

34 Theurl I, Hilgendorf I, Nairz M, *et al*. On-Demand erythrocyte disposal and iron recycling requires transient macrophages in the liver. *Nat Med* 2016;22:945–51.

35 Kina T, Ikuta K, Takayama E, *et al*. The monoclonal antibody TER-119 recognizes a molecule associated with glycophorin A and specifically marks the late stages of murine erythroid lineage. *Br J Haematol* 2000;109:280–7.

36 Liu Z, Gu Y, Chakarov S, *et al*. Fate mapping via Ms4a3-Expression history traces monocyte-derived cells. *Cell* 2019;178:1509–25.

37 Knutson M, Wessling-Resnick M. Iron metabolism in the reticuloendothelial system. *Crit Rev Biochem Mol Biol* 2003;38:61–88. doi:10.1080/713609210

38 Vallelian F, Deuel JW, Opitz L, *et al*. Proteasome inhibition and oxidative reactions disrupt cellular homeostasis during heme stress. *Cell Death Differ* 2015;22:597–611.

39 Olonisakin TF, Suber TL, Gonzalez-Ferrer S. Stressed erythrophagocytosis induces immunosuppression during sepsis through heme-mediated STAT1 dysregulation. *J Clin Invest* 2020;131. [Epub ahead of print: Available from].

40 Vallelian F, Buzzi RM, Pfefferlé M, *et al*. Heme-stress activated NRF2 skews fate trajectories of bone marrow cells from dendritic cells towards red pulp-like macrophages in hemolytic anemia. *Cell Death Differ* 2022;29:1450–65. doi:10.1038/s41418-022-00932-1

41 Long KB, Gladney WL, Tooker GM. Ifnγ and CCL2 cooperate to redirect tumor-infiltrating monocytes to degrade fibrosis and enhance chemotherapy efficacy in pancreatic CarcinomaMonocytes regulate fibrosis in pancreatic carcinoma. *Cancer Discov* 2016;6:400–13. doi:10.1158/2159-8290.CD-15-1032

42 Knorr DA, Dahan R, Ravetch JV. Toxicity of an Fc-engineered anti-CD40 antibody is abrogated by intratumoral injection and results in durable antitumor immunity. *Proc Natl Acad Sci U S A* 2018;115:11048–53.

43 Salomon R, Rotem H, Katzenelenbogen Y, *et al*. Bispecific antibodies increase the therapeutic window of CD40 agonists through selective dendritic cell targeting. *Nat Cancer* 2022;3:287–302.

44 Fransen MF, Sluijter M, Morreau H, *et al*. Local activation of CD8 T cells and systemic tumor eradication without toxicity via slow release and local delivery of agonistic CD40 antibody. *Clin Cancer Res* 2011;17:2270–80.

45 Sum E, Rapp M, Dürr H, *et al*. The tumor-targeted CD40 agonist CEA-CD40 promotes T cell priming via a dual mode of action by increasing antigen delivery to dendritic cells and enhancing their activation. *J Immunother Cancer* 2022;10. doi:10.1136/jitc-2021-003264. [Epub ahead of print: Available from].

46 Salomon R, Dahan R. Next generation CD40 agonistic antibodies for cancer immunotherapy. *Front Immunol* 2022;13:940674.

47 Ye S, Cohen D, Belmar NA, *et al*. A bispecific molecule targeting CD40 and tumor antigen mesothelin enhances tumor-specific immunity. *Cancer Immunol Res* 2019;7:1864–75.

48 Sum E, Rapp M, Fröbel P, *et al*. Fibroblast activation protein α-Targeted CD40 agonism abrogates systemic toxicity and enables administration of high doses to induce effective antitumor immunity. *Clin Cancer Res* 2021;27:4036–53.

Supplemental material

BMJ Publishing Group Limited (BMJ) disclaims all liability and responsibility arising from any reliance placed on this supplemental material which has been supplied by the author(s)

J Immunother Cancer

Pfefferlé et al. - Targeted macrophage reprogramming in the liver

Resource table

Experiment models

Mouse strain	Compagny
C57BL/6J	Charles River
Ms4a3^{Cre}	Prof. Florent Ginhoux (SingHealth and Duke NUS, Singapore)
Ai14^{tdTomato}	Jackson Laboratories
B6.Cg-Tg(TcraTcrb)425Cbn/J (OT-2)	Swiss Immunological Mouse repository (SwImMR)
C57BL/6-Tg(TcraTcrb)1100Mjb/J (OT-1)	Swiss Immunological Mouse repository (SwImMR)
B6.SJL-Ptprca Pepcb/BoyJ (CD45.1)	Swiss Immunological Mouse repository (SwImMR)
LysM^{Cre}	Swiss Immunological Mouse repository (SwImMR)
Clec4f^{cre}	Jackson laboratories
CD40fl/fl	Generated in our laboratory

Tumor cell line	Compagny
GFP^{+} MC38 colon murine adenocarcinoma cells	Obtained from Dr Rok Humar (University Hospital of Zürich, USZ)

Reagents for in vivo or in vitro treatments

Product name	Compagny	Catalogue number
Rat anti-mouse Ter119	InVivoPLus	BE0183
Mouse anti-mouse Ter119	CSL Behring	Not commercialized
IgG2 Isotype Control Antibody	InVivoPlus	BP0085-5MG-R
Rat anti-mouse CD40 agonistic antibody	InVivoPLus	BP0016-2
Etanercept 50 mg (Enbrel) injectable solution	Pfizer	3514981
Rat anti-mouse CD3e antibody	BioXCell	BE001-1
Ketamine	Graeub	QN01AX03
Xylazine	Bayer	QN05CM92
Acepromazine	Fatro	QN05AA04
Lipopolysacharide (LPS) from Escherichia coli O111:B4	Sigma-aldrich	L2630

Antibodies for flow cytometry

Targeted antigen	Clone	Fluorochrome	Specie	Compagny	Identifier
RBC glycophorin protein	TER119	Phycoerythrin (PE)	Rat	Biolegend	116215
F4/80	T45-2342	Allophycocyanin (APC)	Rat	BD	566787
F4/80	T45-2342	Phycoerythrin (PE)	Rat	BD	565410
CD11b	M1/70	APC-Cy7	Rat	Biolegend	101226
CD45	30-F11	Brilliant violet 421	Rat	Biolegend	103134
CD45.1	A20	Brilliant violet 711	Rat	Biolegend	110739
CD45.2	104	Pacific blue	Rat	Biolegend	109820
CD4	GK1.5	Phycoerythrin (PE)	Rat	Biolegend	100408
CD8	53-6.7	Phycoerythrin (PE)	Rat	Biolegend	100708
Rat IgG	-	Alexa Fluor 555	Goat	Invitrogen	A21434
Tru Stain FcxTmPLUS $_{CD16/32}$	S17011E	-	Rat	Biolegend	156604

Primary antibodies for immunofluorescence

Targeted antigen	Clone	Fluorochrome	Specie	Compagny	Identifier
Iba1	Polyclonal	-	Rabbit	Wako	019-19741
F4/80	D2S9R	-	Rabbit	Cellsignal	70076
HMOX1	Polyclonal	-	Rabbit	Enzo	ADI-SPA-896

53

Pfefferle et al. - Targeted macrophage reprogramming in the liver

Secondary antibodies for immunofluorescence

Targeted antigen	Clone	Fluorochrome	Specie	Compagny	Identifier
Anti-rabbit IgG	-	Alexa Fluor 555	Goat	Invitrogen	A-21434
anti-Rabbit HRP	-	HRP	Goat	PerkinElmer	ARR1001KT

Antibodies for single-cell RNA seq with feature barcoding

Targeted antigen	Compagny	Identifier
TotalSeq™ B0301-B0304 Anti-mouse Hashtag antibodies	Biolegend	155831, 155833, 155835, 155837

Fluorescent dyes

Product name	Compagny	Catalogue number
LIVE/DEAD™ Fixable Near-IR Dead Cell Stain Kit	Invitrogen	L10119
Alexa Fluor 488 Phalloidin	ThermoFischer	A12379
CellTrace™ Far Red Cell Proliferation Kit, for flow cytometry (CFSE)	ThermoFischer	C34564
IVISense 680	PerkinElmer	nev12000
Hoechst 33342	ThermoFischer	62249
DAPI spectral solution	PerkElmer	NEL810001KT
Red phRodo Cell Labeling Kit for Incucyte® Phagocytosis Assays	Sartorius	4649
Opal 520 Reagent Pack	Akoya Bioscience	FP1487001KT
Opal 570 Reagent Pack	Akoya Bioscience	FP1488001KT
Opal 620 Reagent Pack	Akoya Bioscience	FP1495001KT

Magnetic beads, magnets and associated antibodies

Product name	Compagny	Catalogue number
Anti-Rat IgG Dynabeads	Invitrogen	11035
Rat anti-mouse F4/80 IgG2a antibodies (clone T45-2342)	BD biosciences	565409
Rat anti-mouse CD11b IgG antibodies (clone M1/70)	Biolegend	101202
DynaMag magnet	Invitrogen	12321D
EasyEights™ EasySep™ Magnet	Stemcell	18103
MagniSort™ Mouse CD4 T cell Enrichment Kit	Invitrogen	8804-6821-74
MagniSort™ Mouse CD8 T cell Enrichment Kit	Invitrogen	8804-6822-74
MagniSort™ Mouse CD45 Positive Selection Kit	Invitrogen	8802-6865-74

Solutions, medium, supplement and enzymes

Product name	Compagny	Catalogue number
Phosphate buffered Saline (PBS)	Gibco	10010-015
HBSS	Gibco	14025092
RPMI-1640 Medium	Gibco	11835-063
Dulbecco's MEM	Merck	1469C
Fetales bovines Serum	Sigma-Aldrich	S0615
L-Glutamine (200 mM)	ThermoFischer	25030024
Sodium-Pyruvate	Sigma	P2256
MEM Non-Essential Amino Acids Solution (100X)	Gibco	11140050
Penicillin-Streptomycin	ThermoFischer	15140-122
Collagenase B	Roche	11088815001
Liberase	Roche	5401119001
Collagenase Type IV	Stemcell	7427
Dnase I	Roche	10269638001
UltraPure™ 0.5M EDTA, pH 8.0	ThermoFisher	15575020

54

Supplemental material

BMJ Publishing Group Limited (BMJ) disclaims all liability and responsibility arising from any reliance
placed on this supplemental material which has been supplied by the author(s)

J Immunother Cancer

Pfefferle et al. - Targeted macrophage reprogramming in the liver

Versene	Gibco	15040066
Calciumchlorid	Sigma-Aldrich	C1016-2.5KG
Percoll plus	Cytiva	GE17-5445-02
RLT Buffer	Qiagen	79216

Peptides, and Recombinant proteins

Product name	Compagny	Catalogue number
EndoFit Ovalbumin (Chicken egg albumin; for in vivo use)	InvivoGen	17E10-MM
Recombinant Murine M-CSF	Peprotech	315-02
20% Human Serum Albumin	CSL Behring AG	3665734
Bovine serum albumin	Newark	16009-13-5
MACS Buffer BSA Stock Solution	Miltenyi Biotec	130-091-376

Chemicals

Product name	Compagny	Catalogue number
Paraformaldehyde (PFA) powder 95%	Sigma-Aldrich	158127
Tween-20	Sigma-Aldrich	P1379
Triton X-100	Sigma-Aldrich	X100
RBC Lysis Buffer (10X)	Biolegend	420301

Critical Commercial Assays

Product name	Compagny	Catalogue number
UltraComp eBeads™ Compensation Beads	ThermoFisher	01-2222-42
Bio-Plex Pro™ Mouse Cytokine ICAM-1 Set	Bio Rad	171GA010M
Bio-Plex Pro™ Mouse Cytokine IL-6 Set	Bio Rad	171G5007M
Bio-Plex Pro™ Mouse Cytokine MCP-1 (MCAF) Set	Bio Rad	171G5019M
Bio-Plex Pro™ Mouse Cytokine MIP-1β Set	BioRad	171G5021M
Bio-Plex Pro™ Mouse Cytokine RANTES	BioRad	171G5022M
Bio-Plex Pro™ Mouse Cytokine TNF-α Set	Bio Rad	171G5023M
Bio-Plex Pro™ Mouse Cytokine IL-12 (p70)	Bio Rad	171G5011M
Bio-Plex Pro™ Mouse Cytokine IL-12 (p40)	Bio Rad	171G5010M
Bio-Plex Pro™ Mouse Cytokine Standards Group I	Bio Rad	171I50001
Bio-Plex Pro™ Mouse Cytokine Standards Group III	Bio Rad	171IA0001
Opal 4 color anti-Rabbit Manual IHC Kit	Akoya Biosciences	NEL840001KT
AR6 Buffer	PerkinElmer	AR600250ML
Antibody block solution	PerkinElmer	ARD1001EA
Antibody diluent	PerkinElmer	ARD1001EA
Opal Polymer anti-Rabbit HRP	PerkinElmer	ARR1001KT
Opal Polymer anti-Rabbit HRP Diluent	PerkinElmer	ARR1001KT
ProLong™ Gold Antifade Mountant	ThermoFisher	P36930
VECTASTAIN® Elite ABC-HRP Kit, Peroxidase (Rabbit IgG)	Vector Laboratories	PK-6101
Chromium Next GEM Single Cell 3' Kit v3.1, 4 rxns	10x Genomics	PN-1000269
DynabeadsTM MyOneTM SILANE	10x Genomics	PN-2000048
3' Feature Barcode Kit, 16 rxns	10x Genomics	PN-1000262
Dual Index Kit TT Set A, 96 rxns	10x Genomics	PN-1000215
Chromium Next GEM Chip G Single Cell Kit, 16 rxns	10x Genomics	PN-1000127
SYBR™ Green Master Mix	Applied Biosystems	4385612
RNeasy Mini Kit	Qiagen	74106
TaqMan reverse transcription reagents	Life Technologies	N8080234

55

Pfefferle et al. - Targeted macrophage reprogramming in the liver

Plates and coating

Product name	Compagny	Catalogue number
96-well plates	Techno Plastic Products (TPP)	Z707902-108EA
70 µm cell strainer filters	Corning	CLS431751
Geltrex™ LDEV-Free Reduced Growth Factor Basement Membrane Matrix	ThermoFischer	A1413302
Insyte-W Catheter I.V. 24G 0,7x19mm	BD	381312

Software

Product name	Compagny
JMP 15	SAS
Prism 9	Dotmatics
R (v4.2.1)	R Foundation for Statistical Computing
Qupath (v0.3.2)	Open Souurce, University of Edinburgh
FlowJo (v10.7.1)	BD
FCS Express 6	De Novo software
7500 Fast System Sequence Detection Software (v1.4)	Applied Biosystems
SingleCell Bbrowser (v3.3.15)	Bioturing

56

Supplemental material

BMJ Publishing Group Limited (BMJ) disclaims all liability and responsibility arising from any reliance
placed on this supplemental material which has been supplied by the author(s)

J Immunother Cancer

Pfefferle et al. - Supplementary Figures

Antibody-induced erythrophagocyte reprogramming of Kupffer cells prevents anti-CD40

cancer immunotherapy-associated liver toxicity

Marc Pfefferlé[1], Irina L Dubach[1], Raphael M Buzzi[1], Elena Dürst[1], Nadja Schulthess-Lutz[1], Livio Baselgia[1], Kerstin Hansen[1], Larissa Imhof[1], Sandra Koernig[2], Didier Le Roy[3], Thierry Roger[3], Rok Humar[1], Dominik J Schaer[1] and Florence Vallelian[1]
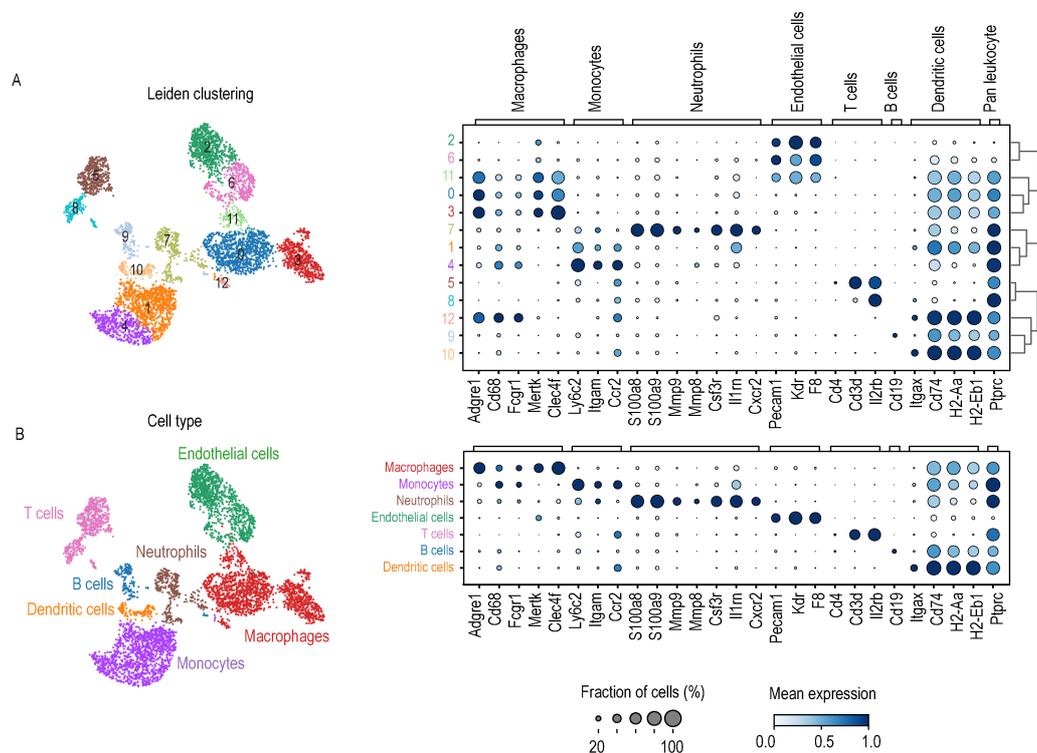
[1]Division of Internal Medicine, University Hospital and University of Zurich, Zurich, Switzerland

[2]CSL Ltd., Research, Bio21 Institute, Parkville, Vic, Australia

[3]Infectious Diseases Service, Lausanne University Hospital and University of Lausanne,

Supplementary Figures

Supplemental material

BMJ Publishing Group Limited (BMJ) disclaims all liability and responsibility arising from any reliance placed on this supplemental material which has been supplied by the author(s)

J Immunother Cancer

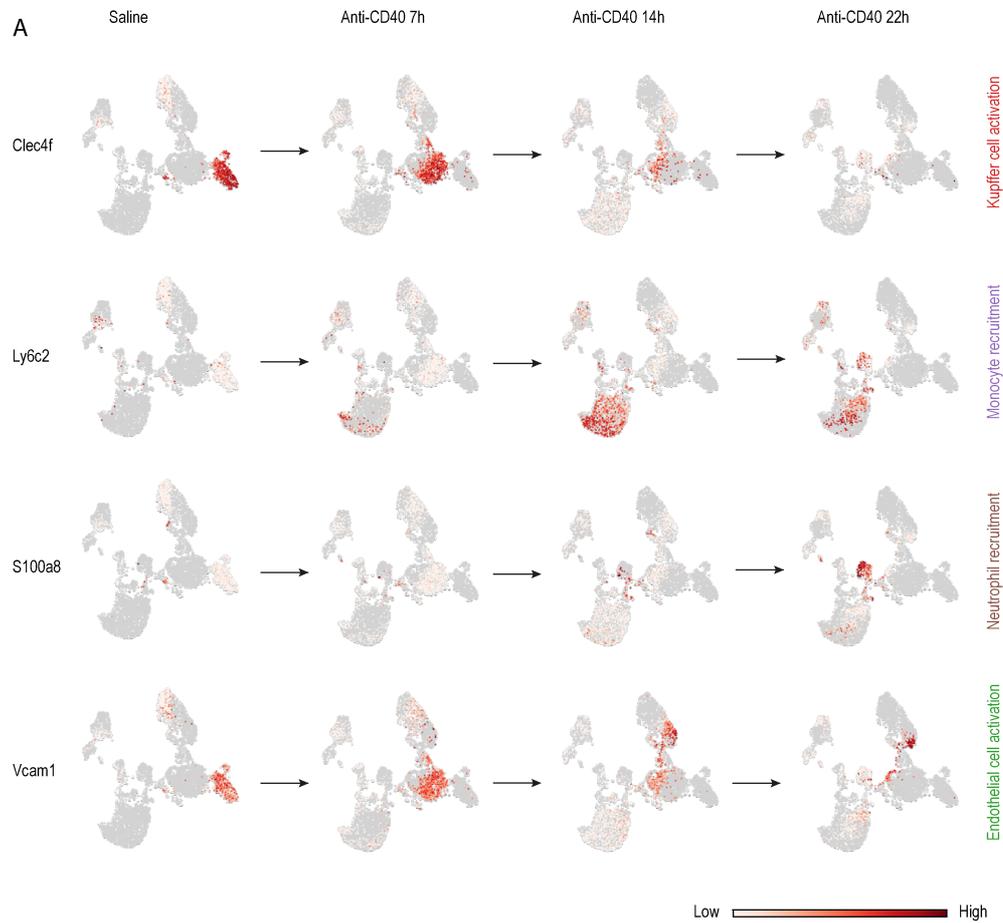Pfefferle et al. - Supplementary Figures

Supplementary Figure 1

Multiplexed sc-RNA-seq experiment performed with wild-type mice that were injected i.v. with an anti-CD40 mAb or saline (0 hours). After 7, 14 and 22 hours, livers were digested into single-cell suspensions and enriched for leukocytes using CD45-coated magnetic beads.

A. Left: UMAP plot with cells colored by clusters as determined by the Leiden unsupervised clustering algorithm. Right: Dot plot displaying the scaled expression of canonical marker genes for each cluster and the proportion of cells expressing the genes.

B. Left: UMAP plot with cells colored by cell identity as determined by the expression of canonical marker genes by each cluster. Right: Dot plot displaying the scaled expression of canonical marker genes for each cell type and proportion of cells in each cell type expressing the genes.

Pfefferle et al. - Supplementary Figures

Supplementary Figure 2

Multiplexed sc-RNA-seq experiment performed with wild-type mice that were injected i.v. with an anti-CD40 mAb (20 mg/kg) or saline (0 hours). After 7, 14 and 22 hours, livers were digested into single-cell suspensions and enriched for leukocytes using CD45-coated magnetic beads.

A. UMAP plots with cells colored based on Clec4f, Ly6c2, S100a8, or Vcam1 expression levels separated by treatment condition (saline or anti-CD40 mAb 7, 14 and 22 hours post injection). The cells are superposed on the gray outline of cells from all conditions.
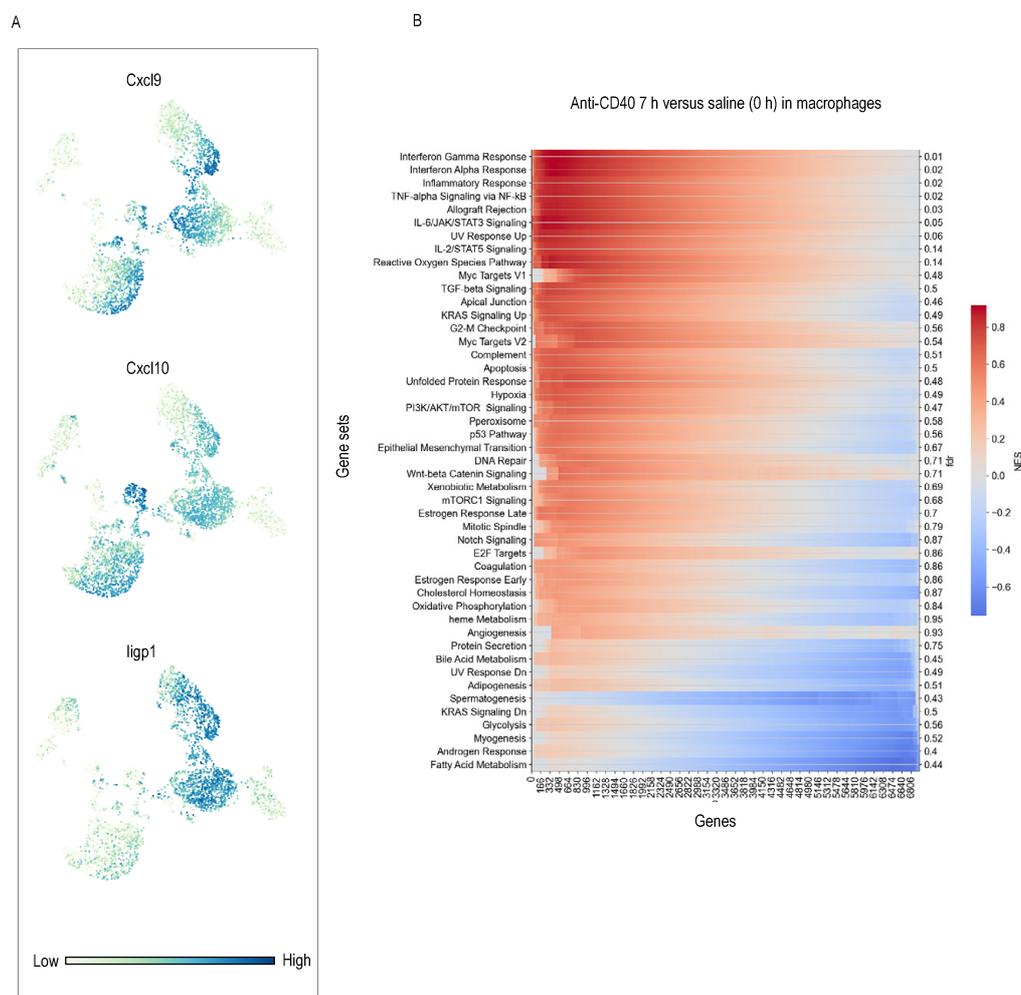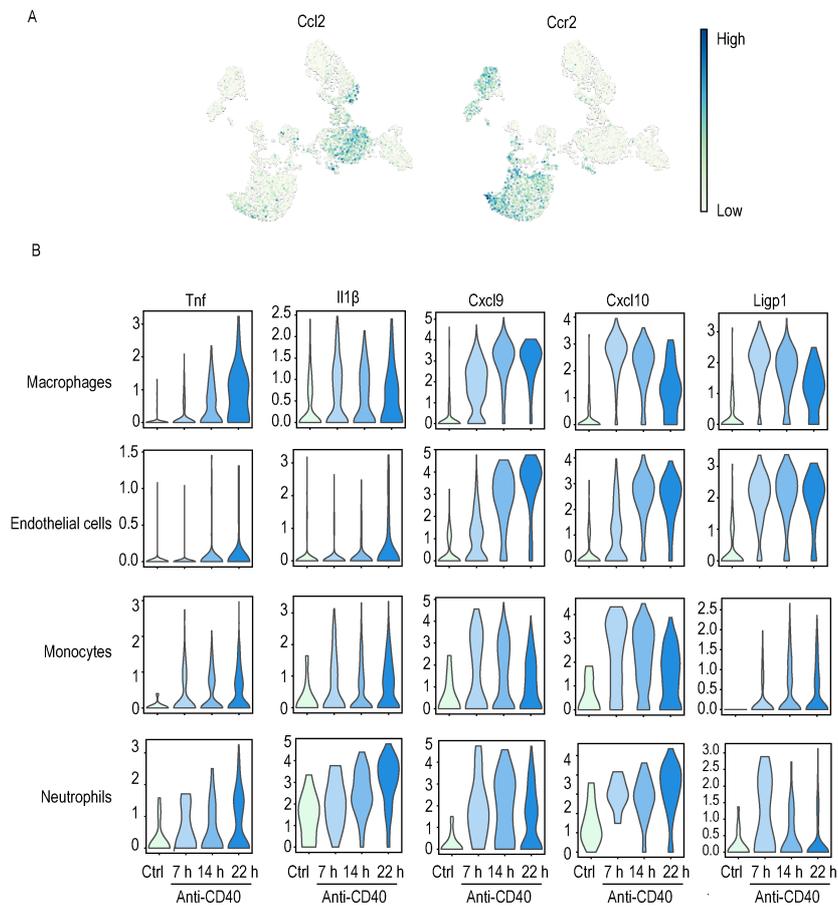
Pfefferle et al. - Supplementary Figures

Supplementary Figure 3

Multiplexed sc-RNA-seq experiment performed with wild-type mice that were injected i.v. with an anti-CD40 mAb or saline (0 hours). After 7, 14 and 22 hours, livers were digested into single-cell suspensions and enriched for leukocytes using CD45-coated magnetic beads.

A. UMAP plots with cells from all conditions colored based on Cxcl9, Cxcl10, or Iigp1 expression levels.

B. Heatmap displaying the results of GSEA of genes differentially expressed between liver macrophages from anti-CD40 mAb-treated mice at 7 h post-treatment and those from saline-treated mice (0 h). The analysis was performed using hallmark gene sets from the Molecular Signature Database (MSigDB). Rows represent individual gene sets and are ordered by normalized enrichment score (NES). The heatmap displays the magnitude of the running enrichment score per gene set category (red = positive enrichment, blue = negative enrichment).

Pfefferle et al. - Supplementary Figures

Supplementary Figure 4

Multiplexed sc-RNA-seq experiment performed with wild-type mice that were injected i.v. with an anti-CD40 mAb or saline (0 hours). After 7, 14 and 22 hours, livers were digested into single-cell suspensions and enriched for leukocytes using CD45-coated magnetic beads.

A. UMAP plots with cells from all conditions colored based on Ccl2 (left) or Ccr2 (right) expression levels.

B. Violin plots displaying the expression levels of Tnf, Il1b, Cxcl9, Cxcl10, and Iigp1 in macrophages, endothelial cells, monocytes, and neutrophils from mice treated with anti-CD40 (7, 14 or 22 h post-anti-CD40 treatment) or saline (Ctrl).
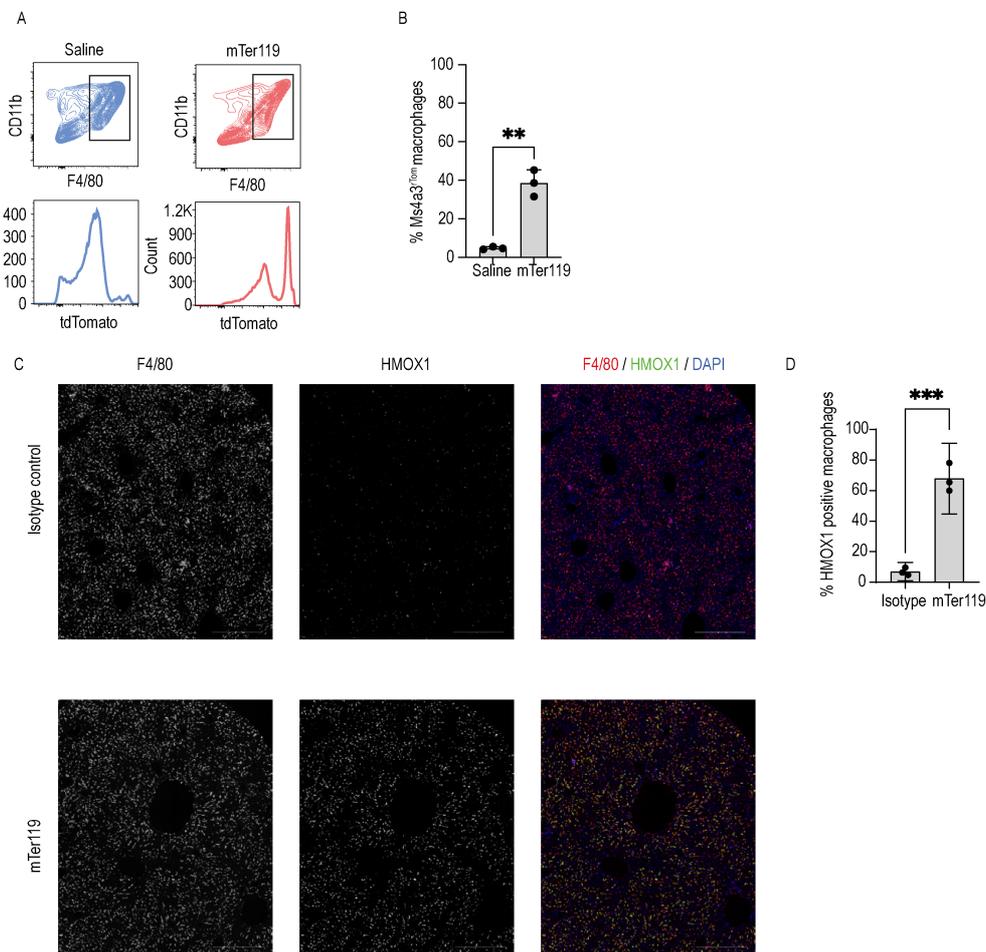
Supplementary Figure 5

A. Top: Flow cytometry contour plots of liver cell suspensions from mTer119-treated (red) or saline-treated (blue) Ms4a3^{Cre}-Rosa^{TdT} mice. The cells were stained for F4/80 and CD11b and gated from live CD45$^+$ cells. Bottom: histogram displaying the intensity of the tdTomato channel (Ms4a3) in F4/80$^+$ cells gated as shown in the contour plots above. The cells were run on a spectral flow cytometer.

B. Cumulative data for the percentage of Ms4a3$^+$ cells in CD45$^+$F4/80$^+$ cells from the liver cell suspensions of mice treated as described in A (each treatment n= 3).

C. Representative multispectral immunofluorescence images of paraffin-embedded liver sections from mTer119- and isotype control-treated C57BL/6 mice. Liver sections were stained with F4/80 (red) and HMOX1 (green) antibodies. Nuclei were counterstained with DAPI (blue). Images were acquired using a Phenolmager HT (Akoya). Scale bar 500 μm.

D. Percentage of HMOX1 and F4/80 double positive cells quantified from stained whole-liver sections of C57BL/6 mice subjected to mTer119 (n = 3) or isotype control treatment (n = 3). Slides were stained as described in C.
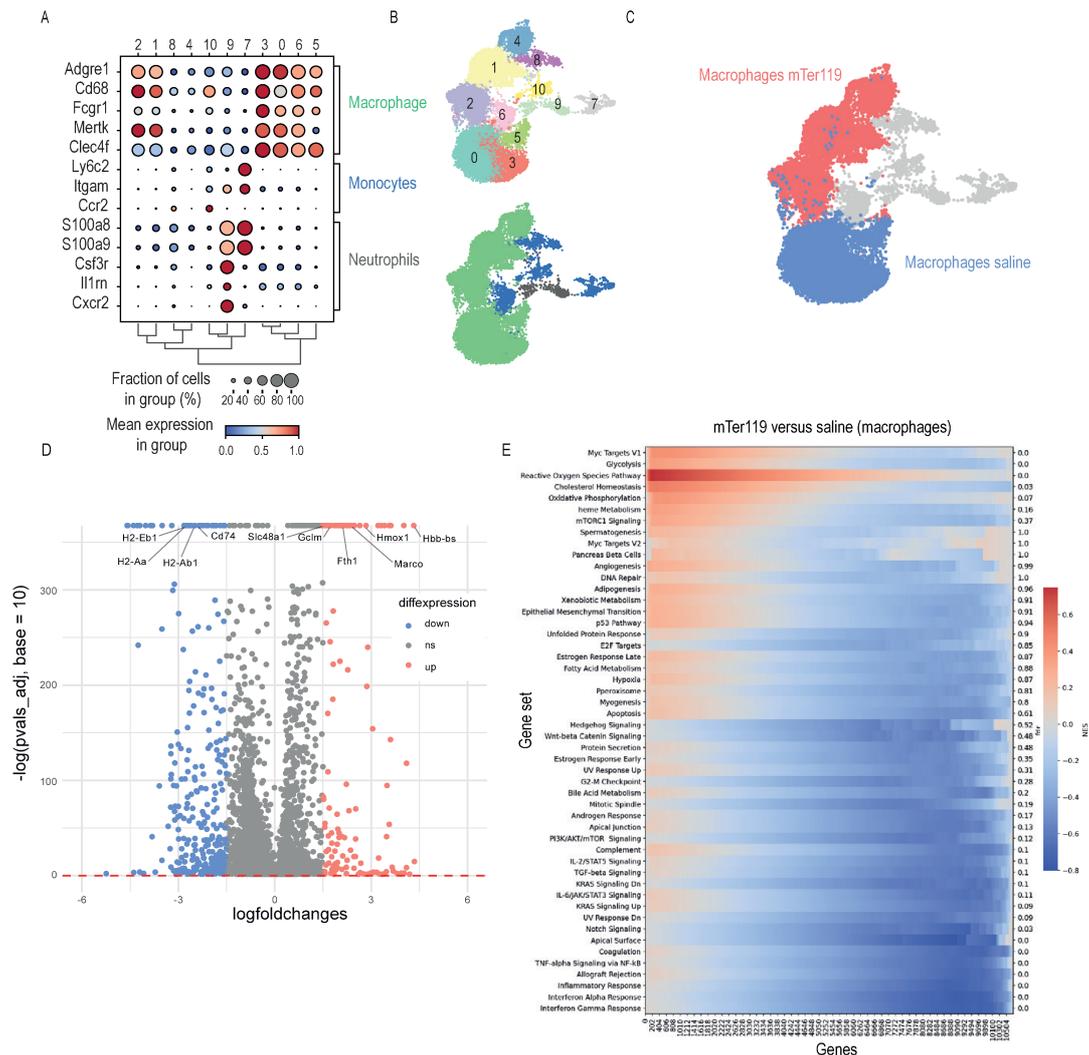
Supplementary Figure 6

Pooled sc-RNA-seq data from two sequencing experiments performed with liver cell suspensions from mTer119- and saline-treated mice. Before sequencing, the liver cells were enriched for macrophages using anti-F4/80- and anti-CD11b-coated magnetic beads. The dataset was subsetted to contain only phagocytes as outlined in Figure 3.

A. Dot plot displaying the scaled expression of canonical marker genes for each cell type and the proportion of cells in each cluster expressing those genes.

B. Top: UMAP plot displaying cells colored by clusters. Bottom: UMAP plot displaying cells colored by cell type. The colors indicate the marker gene-derived cell-type attribution delineated in A.

C. UMAP plot displaying cells with only macrophages highlighted, differentially colored depending on treatment (mTer119 or saline).

D. Volcano plot displaying the results of the differential gene expression analysis between liver macrophages from mTer119- versus saline-treated mice. Key genes related to the erythrophagocyte phenotype are highlighted.

Pfefferle et al. - Supplementary Figures

E. Heatmap presenting the results of gene set enrichment analysis (GSEA) of differentially expressed genes between liver macrophages from mTer119- and saline-treated mice. The analysis was performed using hallmark gene sets from the Molecular Signature Database (MSigDB). Rows represent individual gene sets and are ordered by normalized enrichment score (NES). The heatmap displays the magnitude of the running enrichment score per gene set category (red = positive enrichment, blue = negative enrichment).

Pfefferle et al. - Supplementary Figures
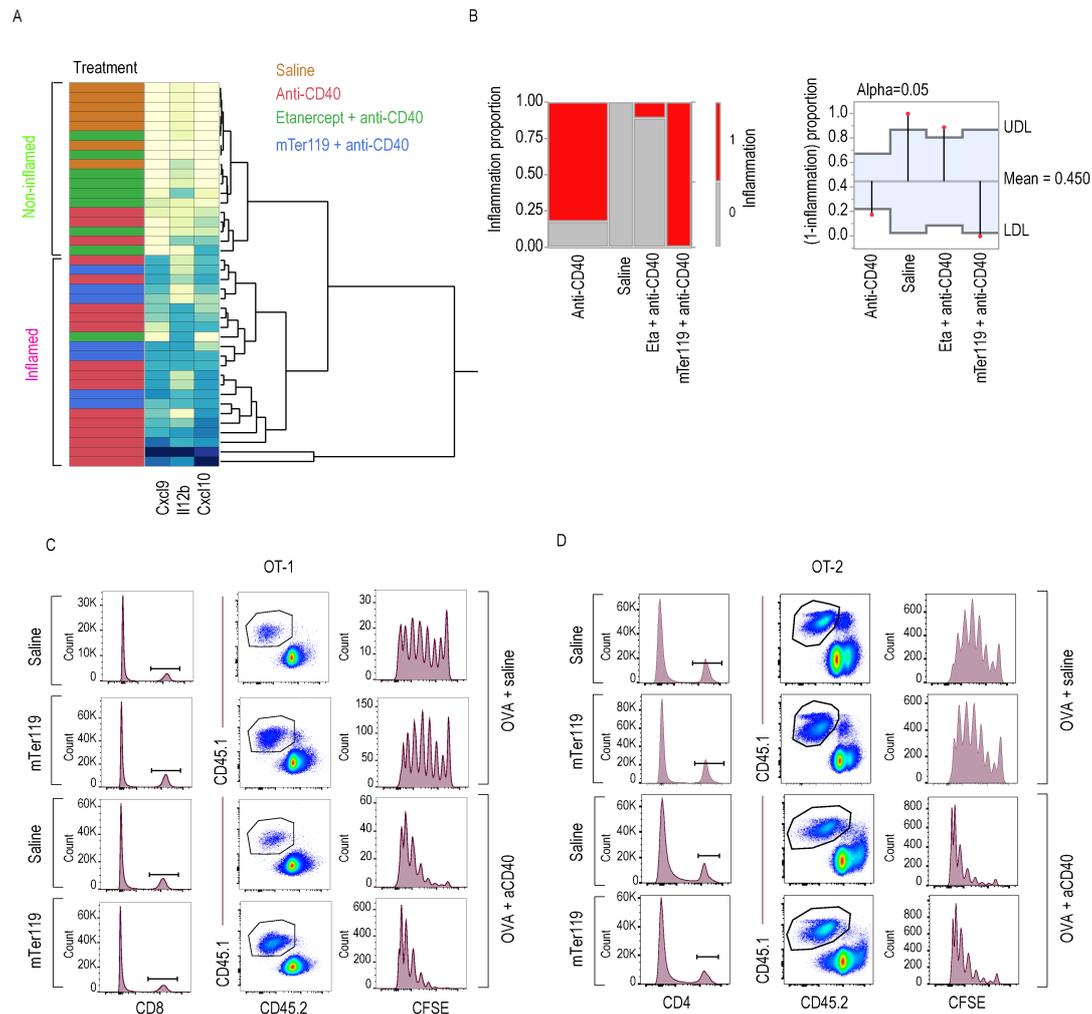
Supplementary Figure 7

A. Heatmap showing unsupervised hierarchical clustering analysis of Cxcl9, Cxcl10 and Il12b gene expression in peritoneal macrophages from C57BL/6 mice subjected to mTer119 (blue), etanercept (green), or saline (red) and challenged with and anti-CD40 mAb (20mg/kg i.p.) or saline (orange). Peritoneal cells were harvested after 16 h and enriched for macrophages with anti-F4/80-coated magnetic beads, and gene expression was measured by RT–qPCR (yellow = low expression, blue = high expression). The clustering analysis classified animals into the inflamed and noninflamed groups.

B. Left: Stacked bar plot displaying the proportion of mice with inflamed peritoneal macrophages from each condition described in A. Red indicates inflamed, gray indicates not inflamed. Right: Proportion data were analyzed by a chi^2 test (p<0.001); displayed is the analysis of means (ANOM) of the four groups (LDL= lower decision line, UDL= upper decision line; defining the confidence intervals).

C. Representative CFSE dilution profiles of adoptively transferred CD8$^+$ T cells in mTer119- or saline-treated mice injected with OVA or OVA+anti-CD40 as described in Figure 5C.

Pfefferle et al. - Supplementary Figures

Representative data for cells gated based on positive CD8 and CD45.1 expression are shown.

D. Representative CFSE dilution profiles of adoptively transferred CD4$^+$ T cells in mTer119- or saline-treated mice injected with OVA or OVA+anti-CD40 as described in Figure 5C. Representative data for cells gated based on positive CD4 and CD45.1 expression are shown.

Pfefferle et al. - Supplementary Figures
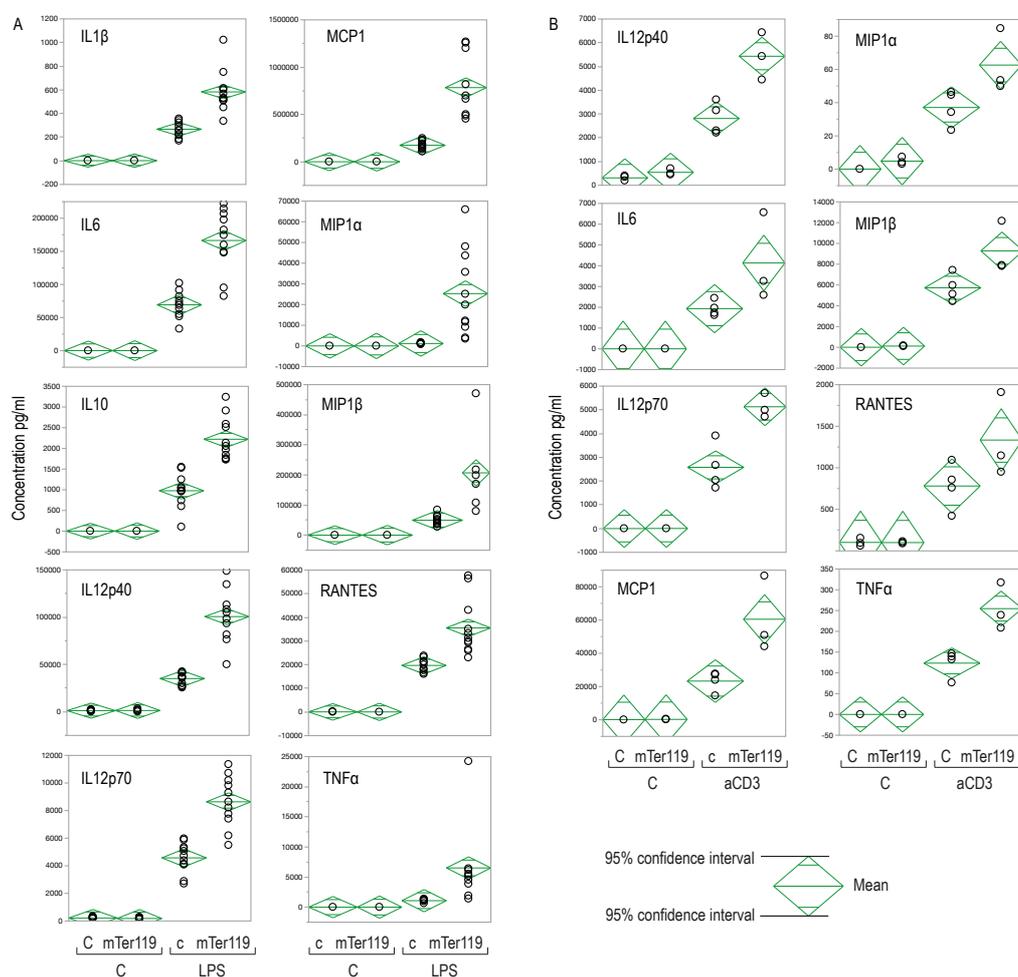
Supplementary Figure 8

A. Diamonds displaying the same data as in Figure 5A of the main manuscript. C57BL/6 mice were treated with mTer119 or saline and injected i.p. with LPS (6 mg/kg). Blood was sampled before (0 hours) and 4 hours after the LPS injection to measure cytokine levels. Every point represents a mouse (n = 11-12 for LPS).

B. Diamonds displaying the same data as in Figure 5B of the main manuscript. C57BL/6 mice were treated with mTer119 or saline and injected i.v. with an anti-CD3 antibody (100 µg). Four hours later, the animals were sacrificed, and blood was collected for proinflammatory cytokine measurement (n = 3-4)

Each dot represents one mouse. The green diamonds represent mean and 95% confidence intervals as indicated in the figure.

Pfefferlé et al. - Supplementary Methods

Antibody-induced erythrophagocyte reprogramming of Kupffer cells prevents anti-CD40 cancer immunotherapy-associated liver toxicity

Marc Pfefferlé[1], Irina L Dubach[1], Raphael M Buzzi[1], Elena Dürst[1], Nadja Schulthess-Lutz[1], Livio Baselgia[1], Kerstin Hansen[1], Larissa Imhof[1], Sandra Koernig[2], Didier Le Roy[3], Thierry Roger[3], Rok Humar[1], Dominik J Schaer[1] and Florence Vallelian[1]

[1]Division of Internal Medicine, University Hospital and University of Zurich, Zurich, Switzerland
[2]CSL Ltd., Research, Bio21 Institute, Parkville, Vic, Australia
[3]Infectious Diseases Service, Lausanne University Hospital and University of Lausanne,

Supplementary Methods (detailed procedures and protocols)

Mice

C57BL/6J (JAX™ strain) mice were obtained from Charles River Laboratories. Ms4a3^{Cre} mice were obtained from Dr. Florent Ginhoux (SingHealth and Duke NUS, Singapore) [1] and bred with Ai14^{tdTomato} mice (The Jackson Laboratory). C57BL/6-Tg(TcraTcrb)1100Mjb/J (OT-1), B6.Cg-Tg(TcraTcrb)425Cbn/J (OT-2), and B6.SJL-Ptprca Pepcb/BoyJ (CD45.1) mice were obtained from the Swiss Immunological Mouse repository (SwImMR). CD45.1 x OT-1 and CD45.1 x OT-2 mice were obtained by crossing OT-1 and OT-2 mice with CD45.1 mice, respectively. The CD40$^{fl/fl}$ mouse strain was generated from the ES clone EPD0901_3_A02, obtained from the KOMP repository (www.komp.org), by the Wellcome Trust Sanger Institute (WTSI) as described previously [2]. CD40$^{fl/fl}$ mice were crossed with Lysm^{Cre} mice, which were obtained from SwImMR, to generate CD40$^{fl/fl}$ LysM^{Cre} mice or with Clec4f^{Cre} mice, which were acquired from The Jackson Laboratory, to obtain CD40$^{fl/fl}$ Clec4f^{Cre} mice. Control littermates without the Cre driver were used for experiments involving these mouse strains.

All breeding colonies were housed and bred in the specific pathogen-free (SPF) animal facility at the Laboratory Animal Services Center (LASC) of the University of Zurich in individually ventilated cages. Mice were housed under a 12/12-h light/dark cycle in accordance with international guidelines. Mice that were 7-10 weeks old were used for all experiments. Only healthy, well-conditioned mice with uncompromised and groomed fur were included as

1

Pfefferle et al. - Supplementary Methods

experimental animals. The mice were monitored daily for health parameters, including weight, in accordance with guidelines provided by the Swiss Federal Veterinary Office.

For all experiments, the experimental unit is defined as a single animal. Both male and female animals were included. All experimental protocols were reviewed and approved by the Veterinary Office of the Canton of Zurich (ZH044 2021). Animal experiments performed in Lausanne were approved by the Service des Affaires Vétérinaires, Direction Générale de l'Agriculture, de la Viticulture et des Affaires Vétérinaires, état de Vaud (Epalinges, Switzerland) under authorizations VD3760b. All animal experiments were performed according to Swiss and ARRIVE guidelines.

In vivo treatments

Ter119 antibodies: Rat anti-mouse Ter119 IgG2 mAb was acquired from InVivoPlus and diluted in sterile phosphate-buffered saline (PBS) before s.c. injection. Murine Ter119 (mTer119) IgG2 mAb was produced by CSL Behring [3] (non commercialized) and diluted in sterile PBS before s.c. injection.

IgG2 Isotype Control Antibody: mouse IgG2a isotype control antibodies were purchased from InVivoPlus and diluted in sterile PBS before s.c. injection. Isotype control antibodies were always injected with a similar dose as mTer119 antibodies.

Transfusion experiments: In total, 10^9 murine RBCs were stained with CFSE (Thermo Fisher, for flow cytometric analysis and histology) or IVISense 680 (PerkinElmer, for in vivo imaging system (IVIS) analysis) for 20 minutes in PBS, washed and opsonized with the rat Ter119 antibody (667 µg/ml). Approximately 150 million RBCs were then injected intravenously into C57BL/6J mice. Blood was collected every 10 minutes for flow cytometric analysis. After 45 minutes, mice were anesthetized by intraperitoneal injection of ketamine (80 mg/kg), xylazine (16 mg/kg), and acepromazine (3 mg/kg), transcardially perfused using 20 ml PBS and organs collected for IVIS analysis. Another group of mice was sacrificed after 1 hour, their liver collected and digested as indicated in the corresponding subsection for flow cytometric analysis or histology.

2

Pfefferle et al. - Supplementary Methods

Prolonged mTer119 treatment: An initial dose of 1.4 mg/kg Ter119 antibody was injected subcutaneously before starting daily s.c. injections of 0.4 mg/kg Ter119 antibody 4 days later for 10 days in total. Analysis or further inflammatory challenges were performed 24 hours after the last injection.

Etanercept treatment: Etanercept was purchased from Pfizer (Enbrel) and injected intraperitoneally (i.p.) into mice at a dose of 100 mg/kg two times before anti-CD40 challenge (days -2 and 0).

Agonistic anti-CD3 antibody challenge: Anti-CD3 antibodies were purchased from BioXCell (clone 145-2C11), diluted in PBS and injected intravenously at a dose of 100 µg in a volume of 2.5 µl/g weight. The animals were sacrificed 4 hours later for plasma cytokine measurements.

LPS challenge: LPS was purchased from Sigma–Aldrich, diluted in PBS and injected i.p. at a dose of 6 mg/kg in a volume of 5 µl/g weight. Blood was sampled before LPS injection and 4 hours after injection for cytokine measurements.

Tumor experiments: MC38 tumor cells were cultured in RPMI medium supplemented with 10% fetal bovine serum (FBS), 1% penicillin/streptomycin, 1% non essential amino acids (NEAA) and 1% sodium-pyruvate (tumor cell culture medium) in 15-cm cell culture dishes (TPP). The cell line was regularly tested for mycoplasma. Once confluent, tumor cells were harvested using Versene 1x (Gibco) (4 min at 37°C), washed twice in PBS, and 3 million tumor cells in 150 µl of culture medium mixed with 150 µl Geltrex (Thermo Fisher) were injected subcutaneously into the mouse flanks (day 0). mTer119 treatment was initiated 7 days before tumor cell injection (day -7) and continued daily for the entire duration of the experiment. Anti-CD40 treatment was administered two times, at day 7 and 9 after tumor cell injection. Tumor volume was measured one day before anti-CD40 treatment and monitored regularly until the end of the experiment on day 15. Tumor dimensions were measured under light isoflurane anesthesia using a caliper, and tumor volume was calculated as $V = (W^2 \times L)/2$, where W is the width and L is the length of the tumor.

Supplemental material

BMJ Publishing Group Limited (BMJ) disclaims all liability and responsibility arising from any reliance placed on this supplemental material which has been supplied by the author(s)

J Immunother Cancer

Pfefferle et al. - Supplementary Methods

Organ and cell preparation

Spleen cell suspensions

Spleens were harvested, mechanically disrupted in PBS and passed through a 70-μm cell strainer. The cell suspensions were then centrifuged (300 xg, 5 min at 4°C), incubated in RBC lysis buffer (BioLegend) for 2 minutes at 37°C and centrifuged once more to obtain spleen cell populations devoid of mature erythrocytes.

Liver digestion

Mice were anesthetized by intraperitoneal injection of ketamine (80 mg/kg), xylazine (16 mg/kg), and acepromazine (3 mg/kg), and the abdomen was cut open to access the portal vein. A 24-G catheter was placed in the portal vein and connected to a pump. The inferior vena cava was cut open to prevent pressure build-up. The liver was perfused through the catheter with 15 ml of HBSS + 2 mM EDTA to clear the blood followed by 50 ml of HBSS + 350 mg of $CaCl_2$ + 0.4 mg/ml collagenase B buffered solution (Roche). After digestion, the liver was excised, mechanically disaggregated in a petri dish on ice, and filtered through a 70-μm-pore cell strainer. The cell suspension was centrifuged once (100 ×g, 3 min at 4°C), and the pellet was discarded. The supernatant was then centrifuged once more (300 ×g, 5 min at 4°C) to obtain a pellet consisting of nonparenchymal cells including liver macrophages.

Colon digestion

The colon was dissected out, and the feces were removed by flushing with HBSS + 10% FBS. The colon was then cut into pieces and placed in a shaker at 37°C for 15 minutes in 50 ml of HBSS + 2 mM EDTA. The supernatant was removed, and the process was repeated 2 more times to remove any adipose tissue. The tissue was then transferred to 5 ml of digestion medium, which consisted of RPMI medium + 10% FBS (Biochrome) + 125 μg/0.65 U Liberase (Roche) + 200 μg/400 U DNase I (Roche), and incubated for 30 minutes on a shaker at 37°C. The digested tissue was then passed through a 70-μm cell strainer and centrifuged (300 ×g, 5 min at 4°C).

Lymph node digestion

The inguinal lymph nodes were dissected out, minced into pieces of approximately 1 mm^3 and incubated in digestion medium (collagenase IV 1%, DNase I 0.04%) on a shaker for 30

4

minutes at 37°C. The digested lymph nodes were then passed through a 70-µm cell strainer and centrifuged (300 ×g, 5 min at 4°C).

Peritoneal cell isolation

Peritoneal lavage was performed by flushing fluid in the peritoneal cavity using a 24-G needle with a 5-ml syringe filled with PBS + 3% FBS (Biochrome). The peritoneal lavage fluid was then passed through a 70-µm cell strainer and centrifuged (300 ×g, 5 min at 4°C).

Macrophage isolation

Anti-rat IgG Dynabeads (Invitrogen) were washed and incubated with rat anti-mouse F4/80 IgG2a antibodies (BD Biosciences) at a ratio of 2.5 µg of antibody per 50 µl of Dynabeads. Single-cell suspensions isolated from the liver, colon or peritoneal cavity were incubated with anti-F4/80-coated Dynabeads on a shaker at 4°C for 30 minutes. After incubation, positive selection of Dynabead-bound single-cell suspensions was performed on a DynaMag magnet (Invitrogen) with three washing steps, as instructed by the manufacturer.

CD4⁺ and CD8⁺ T-cell isolation

CD4⁺ and CD8⁺ T cells were negatively enriched from spleen single-cell suspensions using a MagniSort CD4 or CD8 enrichment kit (Invitrogen) according to the manufacturer's instructions.

RBCs isolation

Blood was collected by heart puncture, applied over 5 ml of Percoll (Cytiva) 70% in a 50 ml Falcon tube and centrifuged at 800 xg 20 minutes at room temperature without brake. After centrifugation, the supernatant was discarded and the RBCs were washed with 50 ml PBS 3000 xg 10 min at 4°C.

CFSE labeling

RBCs, CD4⁺ and CD8⁺ T cells were labeled with a 1 µM CFSE (Thermo Fisher) at 37°C for 20 minutes, washed with PBS and counted before use. The final purity of T cells was confirmed to be > 95% by flow cytometry.

Pfefferle et al. - Supplementary Methods

Adoptive transfer experiments

In total, 10^6 CFSE-labeled CD4$^+$ T or CD8$^+$ T cells isolated from spleens harvested from CD45.1 x OT-2 or CD45.1 x OT-1 mice, respectively, were injected intravenously into chronic mTer119- or saline-treated mice. After two hours, the mice were challenged intravenously with 75 µg of OVA protein (InvivoGen) in combination with 75 µg of agonistic anti-CD40 mAbs administered subcutaneously to both flanks. After 72 hours, the mice were sacrificed, the draining iliac lymph nodes were harvested as described above, and the CFSE dilution of CD45.1$^+$CD4$^+$ or CD45.1$^+$CD8$^+$ T cells was assessed by flow cytometry.

Plasma cytokine and transaminase measurements

Blood was collected by terminal heart puncture under anesthesia or submental blood sampling and centrifuged at 3000 ×g for 10 minutes at 4°C to obtain the plasma. Plasma cytokine measurements were then performed with diluted plasma (1:5) by using Bio-Plex Cytokine Assays (Bio–Rad) as instructed by the manufacturer. The assays were performed with a Bio-Plex 200 system (Bio–Rad), and the results were analyzed using the Bio-Plex Data Pro software (Bio–Rad) protocol. ALT levels in diluted plasma were measured using a Reflotron (Roche) system as instructed by the manufacturer's protocol.

Flow cytometry

In all flow cytometry experiments, except for flow cytometric analysis of RBCs, live dead staining was performed using the LIVE/DEAD Fixable Near-IR cell stain kit (Invitrogen) as described by the manufacturer. Fc receptor blockade was performed by preincubating cells with TruStain FcX™ PLUS (anti-mouse CD16/32) antibodies (BioLegend). Multiparameter analysis was performed with an LSR Fortessa analyzer (BD Biosciences) or an Aurora 5L spectral flow cytometer (Cytek). The autofluorescence of cells was subtracted in all experiments using a spectral flow cytometer. Data were analyzed using FlowJo software (version 10.7.1) and FCS Express 6 (De Novo software).

IVIS imaging

C57BL/6J mice were transcardially perfused with PBS and imaging of their liver, spleen, kidneys and heart was performed using Program Living Image 4.7.1 software with the

6

Pfefferle et al. - Supplementary Methods

following parameters: excitation wavelength of 640 nm, emission wavelength of 710 nm, exposure time of 2 seconds, binning of 1 and field of view of 10.

Histology (IF and brightfield)

Mice were anesthetized by intraperitoneal injection of ketamine (80 mg/kg), xylazine (16 mg/kg), and acepromazine (3 mg/kg) and transcardially perfused with cold PBS. Organs were fixed by transcardial perfusion of 4% paraformaldehyde (PFA), harvested and placed in 4% PFA.

Organ fixation for paraffin embedding and microtome sectioning
After 12 hours, organs were removed from the 4% PFA solution and embedded in paraffin blocks. Microtome sections (5 µm) were cut for hematoxylin and eosin or IF staining.

Organ fixation for vibratome sections
After 4 hours, organs were removed from the 4% PFA solution, and vibratome sections (70 µm) were cut for IF staining.

IF staining for Vibratome sections

Vibratome sections were permeabilized with 0.5% Triton X-100 in PBS with 4% BSA for 4 hours and then incubated overnight at 4°C with a rabbit anti-mouse Iba1 antibody (WAKO) diluted 1:1000 in PBS containing 0.2% Triton X-100 and 2% BSA, followed by incubation for 2 hours with Alexa Fluor 555-coupled goat anti-rabbit IgG (Invitrogen) diluted 1:400 in PBS containing 0.2% Triton X-100m and 2% BSA. The sections were counterstained with Alexa Fluor 488-conjugated Phalloidin (Thermo Fisher, 1:1000) and Hoechst 33342 (Thermo Fisher, 1:2000) in 0.2% Triton X-100m and 2% BSA for 40 minutes. The sections were washed in PBS after each antibody incubation step and mounted on glass coverslips using ProLong Gold Antifade Mountant (Thermo Fisher).

Multispectral Multiplex Immunofluorescence for paraffin-embedded slides

Paraffin-embedded microtome sections were stained for IF analysis using the Opal 4-Color anti-Rabbit Manual IHC Kit (Akoya Biosciences). Briefly, after 1 h incubation at 65°C, the slides were rehydrated through successive xylol and ethanol incubation steps and further fixed in

7

Pfefferle et al. - Supplementary Methods

10% neutral buffered formalin for 20 minutes. For antigen retrieval, the slides were incubated in boiling pH 6 AR buffer (PerkinElmer) for 30 minutes and then allowed to cool to room temperature for 15-30 minutes. The slides were incubated in Hydrogen Peroxide 0.3% for 10 minutes, then blocked with Antibody Block solution (PerkinElmer) for another 10 minutes and washed in Tris-buffered saline with Tween 20 (TBST). A primary rabbit anti-mouse F4/80 antibody solution (CellSignaling Technologies) was diluted 1:500 in Antibody Diluent (PerkinElmer) and incubated on the slides for 1 hour. The slides were then washed in TBST and incubated for 10 minutes with secondary Opal Polymer anti-Rabbit HRP (PerkinElmer) diluted 1:5 in Opal Polymer anti-Rabbit HRP Diluent (PerkinElmer). After another round of washing with TBST, the slides were incubated with Opal Fluorophore 570 for 10 minutes. The slides were placed in boiling pH 6 AR buffer (PerkinElmer) for 30 minutes to strip off the bound antibodies and allowed to cool for 15 minutes. For F4/80 and HMOX1 co-staining, the slides were subjected to another round of staining using a primary rabbit anti-mouse HMOX1 antibody (ENZO) diluted 1:500 with a 12 hour incubation. In this case the Opal Fluorophore used were 620 for F4/80 and 520 for HMOX1. Finally, the slides were counterstained with a DAPI spectral solution (PerkinElmer) and mounted using ProLong Gold Antifade Mountant (Thermo Fisher).

Microscopy image acquisition and analysis

Whole-liver sections processed by hematoxylin-eosin, immunohistochemical (IHC) or IF staining and embedded in paraffin were acquired using a Zeiss Axio Scan.Z1 microscope or a Akoya Phenoimager HT. Regions of liver vibratome sections subjected to IF staining were visualized with a Leica SP8 confocal laser scanning microscope. Images were analyzed using Qupath [4] (v0.3.2) and ImageJ.

Macrophage quantification in IF tissue sections

F4/80^{+} cells were quantified in whole-liver sections using the integrated watershed cell detection plugin in Qupath. The cells were detected in the Alexa Fluor 555 channel using a requested pixel size of 0.5 μm. The background radius, median filter radius and sigma were 8, 0 and 1.5 μm, respectively. The minimum and maximum areas were 10 and 400 μm^2, respectively. The threshold was set to 150, and cell expansion to 2 μm.

Pfefferle et al. - Supplementary Methods

Quantification of HMOX1 positive macrophages in multiplex IF tissue sections

F4/80^{+} cells and expression of HMOX1 were quantified in whole-liver sections using the integrated positive cell detection plugin in Qupath. F4/80[+] were detected in the Opal 620 channel using the requested pixel size of 0.5 µm. The background radius, median filter radius and sigma were 8, 0 and 1.5 µm, respectively. The minimum and maximum areas were 10 and 500 µm^2, respectively. For intensity parameters split by shape was activated and the threshold was set to 25. Cell expansion was set to 1.5 µm. HMOX1 positive cells were detected using the Opal 520 channel, setting the intensity threshold parameters for score compartment to cytoplasm mean and the threshold to 20.

BMDM cell culture

BM cells were isolated by flushing the femurs and tibias of 8- to 10-week-old C57BL/6J mice, followed by straining of the BM through a 70-µm filter. The BM cells were plated at a density of 30000 cells/cm^2 on tissue culture-treated 96-well plates (TPP) in complete RPMI-1640 medium (10% fetal calf serum (FCS) and 1% L-glutamine) supplemented with 1% penicillin/streptomycin (P/S) and 100 ng/ml recombinant mouse M-CSF (PeproTech). On day 3, half of the medium was replaced. Experiments were carried out on day 7.

In vitro erythrophagocytosis assay

BMDMs were isolated and cultured on a 96-well plate at a concentration of 10^4 cells/well as described above. On day 7 of BMDM culture, donor RBCs were obtained from mice by submental vein puncture. The whole-blood samples were washed twice with PBS. RBCs (50x10^6) were stained using red pHrodo (pHrodo® Cell Labeling Kit for Incucyte® Phagocytosis Assays, Sartorius) according to the manufacturer's protocol. Stained RBCs were added to increasing concentrations of BMDMs. Immediately before starting image acquisition, the Ter119 antibody (400µg/ml) was added to each well. Images were acquired every 15 minutes for 8 hours using an Incucyte®live-cell analysis system.

Sequencing-based workflows and data analysis

scRNA-seq data acquisition

Multiplexed anti-CD40 experiment: Livers from anti-CD40 mAb- and saline-treated mice were digested, and leukocytes were enriched using the MagniSort™ Mouse CD45 Positive Selection

9

Supplemental material

BMJ Publishing Group Limited (BMJ) disclaims all liability and responsibility arising from any reliance placed on this supplemental material which has been supplied by the author(s)

J Immunother Cancer

Pfefferle et al. - Supplementary Methods

Kit (Invitrogen) according to the manufacturer's instruction . Approximately 2 million cells per condition were stained with 1.5 µg of TotalSeq™ B0301-B0304 anti-mouse Hashtag antibodies (BioLegend) in accordance with the manufacturer's instructions and pooled together at equal cell numbers. The pooled multiplexed sample was then processed according to the 10x Genomics Chromium Single Cell 3' v3.1 Reagent Kit with Feature Barcoding Technology for Cell Surface Protein instruction guide (10x Genomics).

mTer119 experiment: Livers from mTer119-treated and saline-treated mice were digested, and macrophages were enriched using a mixture of rat anti-mouse F4/80-coated (BD Biosciences) and rat anti-mouse CD11b (BioLegend)-coated Dynabeads (Invitrogen) for positive selection with direct isolation according to the manufacturer's instructions. The anti-F4/80-coated and anti-CD11b-coated Dynabeads were mixed together at a ratio of 60:40. The enriched cell population was then processed according to the 10x Genomics Chromium Single Cell 3' v3.1 Reagent Kit instruction guide (10x Genomics).

For all experiments, the sample volume was adjusted to a target capture of 10000 cells, and the sample was loaded on the 10x Genomics chromium next-GEM chip G to generate gel beads-in-emulsion (GEMs). The GEM solution was placed in an Applied Biosystems Veriti 96-well thermocycler for reverse transcription, as described by the 10x Genomics instruction guide (53 min at 53°C followed by 5 min at 85°C). The resulting barcoded cDNA was then cleaned using Dynabeads MyOne Silane and amplified for 11 cycles (as recommended by the 10x Genomics user guide for a target cell recovery of >6000 cells). After amplification, for multiplexed experiments, cDNA generated from polyadenylated mRNA for the 3' gene expression library was separated from DNA generated for the Cell Surface Protein Feature Barcode for the Cell Surface Protein library with Dynabeads MyOne Silane and SPRIselect reagents based on size. The quality and concentration of both cDNA and DNA were assessed using a High-Sensitivity D5000 ScreenTape (Agilent). All samples exhibited product sizes with a narrow distribution centered at approximately 2000 bp and yielded between 50 and 800 ng of cDNA (manually selecting products between 100-250 and 5000-6000 bp). cDNA and DNA were then subjected to enzymatic fragmentation, end repair and A-tailing. Adaptors were ligated to the fragmented cDNA and DNA, and the sample index was added during sample index PCR (set for 12 cycles, as recommended by the 10x Genomics user guide to correlate

10

Supplemental material

BMJ Publishing Group Limited (BMJ) disclaims all liability and responsibility arising from any reliance placed on this supplemental material which has been supplied by the author(s)

J Immunother Cancer

Pfefferle et al. - Supplementary Methods

with a cDNA/DNA input of 12-150 ng). Library quality and concentration were assessed using a High-Sensitivity D5000 ScreenTape (Agilent). All gene expression libraries showed an average fragment size of approximately 400 bp. For multiplexed runs, 3' Gene Expression and Cell Surface Protein libraries were pooled at a ratio of 4:1 and sequenced on an Illumina NovaSeq 6000 system with a sequencing depth of 50000 and 12500 reads per cell, respectively, following the recommendations of 10X Genomics (paired-end reads, single indexing, read 1 = 28 cycles, i7 = 8 cycles, i5 = 0 cycles and read 2 = 91 cycles). For nonmultiplexed runs, the 3' Gene Expression libraries for each sample were pooled at an equimolar amount and sequenced on an Illumina NovaSeq 6000 system with a sequencing depth of 50000 reads per cell, following the same recommendations of 10x Genomics.

scRNA-seq data analysis

The Cell Ranger Single-Cell Software Suite (version 6.0.2) was used for cDNA oligopeptide alignment to the reference GRCm38.p5, barcode assignment and UMI counting of fastq files obtained by Illumina sequencing. For each sample, the cell-containing droplets were filtered from the empty droplets, followed by the generation of an expression matrix using Cell Ranger Count (version 6.0.2). Demultiplexing of the cells within each sample was performed with the filtered matrix produced by Cell Ranger in R (version 3.6.3) using Seurat (version 3.2.3) [5] and the HTODemux function (positive quantile set at 0.99). The resulting gene expression matrices were further analyzed with Python (version 3.8.6) using the Scanpy (version 1.7.0) [6] library. Low-quality cells were defined as those with less than 1500 total counts, expressing more than 5000 or fewer than 350 genes or those in which mitochondrial genes accounted for more than 15% of all genes or ribosomal genes accounted for more than 15% of all genes and were excluded from downstream analyses. Genes expressed in fewer than 100 cells were also removed. Normalization was performed using the pool-based size factor estimation implemented in the scran R package (version 1.14.1) [7,8]. Size factors were determined using the function, and normalization was performed by dividing the total gene count in each cell by the cell-specific size factor, deconvoluted from the pool size factor. Data were log transformed. For the Ter119 dataset, the data from the two conditions were integrated using scanorama for batch-effect correction (version 1.7.1) based on the top 5000 DEG. Principal component analysis (PCA) was performed using the tl.pca function (Scanpy 1.7.0) with default settings followed by nearest neighbor graph construction using the pp.neighbors (Scanpy

11

Pfefferle et al. - Supplementary Methods

1.7.0) function with the first 15 principal components. Further dimensionality reduction was performed using the Leiden algorithm, and cells were plotted in 2 dimensions using UMAP plots. Differential gene expression was calculated using the tl.rank_genes_group function (Scanpy 1.7.0) with the implemented Wilcoxon rank sum test. After marker gene based cell type assignment all non-phagocyte cells were excluded from downstream analysis.

RNA-velocity analysis

For the Ter119 dataset, the ratio of spliced and unspliced counts was calculated using velocyto (version 0.17.16) [9]. The resulting matrix was merged with the counts dataset, followed by RNA velocities calculation and visualization using scVelo (version 0.2.3.) [10].

Pathway and transcription factor enrichment analysis of scRNA-seq data

Pathway enrichment analysis was performed using the GSEApy library (version 0.10.7) [11] with hallmark gene sets from the Molecular Signature Database (MSigDB) [12] as a reference. For the input, we used the preranked analysis with all genes ranked according to p value*sign(log fold change). Mus musculus gene names were converted to human gene names using the python based Biomart library (0.9.2) [13]. The pathway enrichment analysis results were visualized using heatmaps, with each row corresponding to a pathway, and the running enrichment score for each gene was plotted. The rows were ordered according to their normalized enrichment score.

RT–qPCR analysis

Total RNA was isolated from liver macrophages using the RNeasy Mini Kit (Qiagen) according to the manufacturer's instructions. TaqMan reverse transcription reagents (Life Technologies) were used for reverse transcription with the following cycling protocol: 10 min at 25°C, 39 min at 48°C and 5 min at 95°C (Mastercycler gradient, Eppendorf, Z316083). RT–qPCR was performed using Fast SYBR™ Green Master Mix (Applied Biosystems) on a 7500 Fast Real-Time PCR System (Applied Biosystems). The primers and their corresponding target genes are listed in Table 2. Relative mRNA levels for experimental samples were calculated with 7500 Fast System Sequence Detection Software version 1.4 (Applied Biosystems) after normalization to *Hprt* levels.

Supplemental material

BMJ Publishing Group Limited (BMJ) disclaims all liability and responsibility arising from any reliance placed on this supplemental material which has been supplied by the author(s)

J Immunother Cancer

Pfefferle et al. - Supplementary Methods

Table 2: Sequences for PCR primers

Target gene	Forward sequence (5'-3')	Reverse sequence (3'-5')
Hprt	cctcctcagaccgcttttt	aacctggttcatcatcgctaa
Cxcl9	gctgccgtcattttctgc	tctcactggcccgtcatc
Cxcl10	cttttcctcttgggcatcat	gcatcgtgcattccttatca
Il12b	tgggagtaccctgactcctg	aggaacgcacctttctggtt
Cd74	caccgaggctccacctaaag	ttaccgttctcgtcgcactt
Hmox1	aggctaagaccgccttcct	tgtgttcctctgtcagcatca

Statistical analysis

Sample size was calculated with R (4.1.2). Data plotting and statistical analysis were performed with Prism 9 (GraphPad) and JMP 15 (SAS) or the Bioturing SingleCell browser (v3.3.15). We used ANOVA with Tukey's posttest, t tests (two-tailed), and Fisher's test or the chi^2 test to analyze contingency tables, as indicated in the figure legends. All data points are displayed in bar plots as the mean ± standard deviation (n.s. = not significant, *$P \leq 0.05$, **$P \leq 0.01$, ***$P \leq 0.001$, ****$P \leq 0.0001$).

Supplemental material

BMJ Publishing Group Limited (BMJ) disclaims all liability and responsibility arising from any reliance placed on this supplemental material which has been supplied by the author(s)

J Immunother Cancer

Pfefferle et al. - Supplementary Methods

REFERENCES

1. Liu Z, Gu Y, Chakarov S, Bleriot C, Kwok I, Chen X, et al. Fate Mapping via Ms4a3-Expression History Traces Monocyte-Derived Cells. Cell. 2019;178:1509–25.e19.

2. Ingoglia G, Yalamanoglu A, Pfefferlé M, Dubach IL, Schaer CA, Valkova K, et al. Line-selective macrophage activation with an anti-CD40 antibody drives a hemophagocytic syndrome in mice. Blood Adv. 2020;4:2751–61.

3. Crow AR, Kapur R, Koernig S, Campbell IK, Jen C-C, Mott PJ, et al. Treating murine inflammatory diseases with an anti-erythrocyte antibody. Sci Transl Med [Internet]. 2019;11. Available from: https://stm.sciencemag.org/content/11/506/eaau8217

4. Bankhead P, Loughrey MB, Fernández JA, Dombrowski Y, McArt DG, Dunne PD, et al. QuPath: Open source software for digital pathology image analysis. Sci Rep. 2017;7:16878.

5. Hao Y, Hao S, Andersen-Nissen E, Mauck WM 3rd, Zheng S, Butler A, et al. Integrated analysis of multimodal single-cell data. Cell. 2021;184:3573–87.e29.

6. Wolf FA, Angerer P, Theis FJ. SCANPY: large-scale single-cell gene expression data analysis. Genome Biol. 2018;19:15.

7. Lun ATL, McCarthy DJ, Marioni JC. A step-by-step workflow for low-level analysis of single-cell RNA-seq data with Bioconductor. F1000Res. 2016;5:2122.

8. Lun ATL, Bach K, Marioni JC. Pooling across cells to normalize single-cell RNA sequencing data with many zero counts. Genome Biol. 2016;17:75.

9. La Manno G, Soldatov R, Zeisel A, Braun E, Hochgerner H, Petukhov V, et al. RNA velocity of single cells. Nature. 2018;560:494–8.

10. Bergen V, Lange M, Peidli S, Wolf FA, Theis FJ. Generalizing RNA velocity to transient cell states through dynamical modeling. Nat Biotechnol. 2020;38:1408–14.

11. Subramanian A, Tamayo P, Mootha VK, Mukherjee S, Ebert BL, Gillette MA, et al. Gene set enrichment analysis: a knowledge-based approach for interpreting genome-wide expression profiles. Proc Natl Acad Sci U S A. 2005;102:15545–50.

12. Liberzon A, Birger C, Thorvaldsdóttir H, Ghandi M, Mesirov JP, Tamayo P. The Molecular Signatures Database (MSigDB) hallmark gene set collection. Cell Syst. 2015;1:417–25.

13. Durinck S, Spellman PT, Birney E, Huber W. Mapping identifiers for the integration of genomic datasets with the R/Bioconductor package biomaRt. Nat Protoc. 2009;4:1184–91.